



Rapid assessment of Watson–Crick to Hoogsteen exchange in unlabeled DNA duplexes using high-power SELOPE imino ^1H CEST

Bei Liu¹, Atul Rangadurai¹, Honglue Shi², and Hashim M. Al-Hashimi^{1,2}

¹Department of Biochemistry, Duke University School of Medicine, Durham, NC, USA

²Department of Chemistry, Duke University, Durham, NC, USA

Correspondence: Hashim M. Al-Hashimi (hashim.al.hashimi@duke.edu)

Received: 10 July 2021 – Discussion started: 20 July 2021

Revised: 20 August 2021 – Accepted: 5 September 2021 – Published: 14 September 2021

Abstract. In duplex DNA, Watson–Crick A–T and G–C base pairs (bp’s) exist in dynamic equilibrium with an alternative Hoogsteen conformation, which is low in abundance and short-lived. Measuring how the Hoogsteen dynamics varies across different DNA sequences, structural contexts and physiological conditions is key for identifying potential Hoogsteen hot spots and for understanding the potential roles of Hoogsteen base pairs in DNA recognition and repair. However, such studies are hampered by the need to prepare ^{13}C or ^{15}N isotopically enriched DNA samples for NMR relaxation dispersion (RD) experiments. Here, using SElective OptimizeD Proton Experiments (SELOPE) ^1H CEST experiments employing high-power radiofrequency fields ($B_1 > 250$ Hz) targeting imino protons, we demonstrate accurate and robust characterization of Watson–Crick to Hoogsteen exchange, without the need for isotopic enrichment of the DNA. For 13 residues in three DNA duplexes under different temperature and pH conditions, the exchange parameters deduced from high-power imino ^1H CEST were in very good agreement with counterparts measured using off-resonance $^{13}\text{C} / ^{15}\text{N}$ spin relaxation in the rotating frame ($R_{1\rho}$). It is shown that ^1H – ^1H NOE effects which typically introduce artifacts in ^1H -based measurements of chemical exchange can be effectively suppressed by selective excitation, provided that the relaxation delay is short (≤ 100 ms). The ^1H CEST experiment can be performed with $\sim 10\times$ higher throughput and $\sim 100\times$ lower cost relative to $^{13}\text{C} / ^{15}\text{N}$ $R_{1\rho}$ and enabled Hoogsteen chemical exchange measurements undetectable by $R_{1\rho}$. The results reveal an increased propensity to form Hoogsteen bp’s near terminal ends and a diminished propensity within A-tract motifs. The ^1H CEST experiment provides a basis for rapidly screening Hoogsteen breathing in duplex DNA, enabling identification of unusual motifs for more in-depth characterization.

1 Introduction

Soon after the discovery of the DNA double helix, it was shown that A–T and G–C could also pair in an alternative conformation known as the “Hoogsteen” base pair (bp) (Felsenfeld et al., 1957; Hoogsteen, 1959) (Fig. 1a). Starting from a canonical Watson–Crick G–C or A–T bp, the corresponding Hoogsteen bp’s can be obtained by flipping the purine base 180° and bringing the two bases into proximity to create a new set of hydrogen bonds, which in the case of G–C bp’s require protonation of cytosine N3 (Fig. 1a).

Following their discovery, Hoogsteen bp’s were observed in crystal structures of duplex DNA in complex with proteins (Kitayner et al., 2010; Aishima et al., 2002) and drugs (Wang et al., 1984; Ughetto et al., 1985) and shown to play a role in DNA recognition (Golovenko et al., 2018), damage induction (Xu et al., 2020), and repair (Lu et al., 2010), and in damage bypass during replication (Nair et al., 2006; Ling et al., 2003). NMR relaxation dispersion (RD) studies employing off-resonance ^{13}C and ^{15}N spin relaxation in the rotating frame ($R_{1\rho}$) later showed that the G–C and A–T Watson–Crick bp’s exist in a dynamic equilibrium with their Hoogsteen counterparts (Nikolova et al., 2011). The Hoogsteen

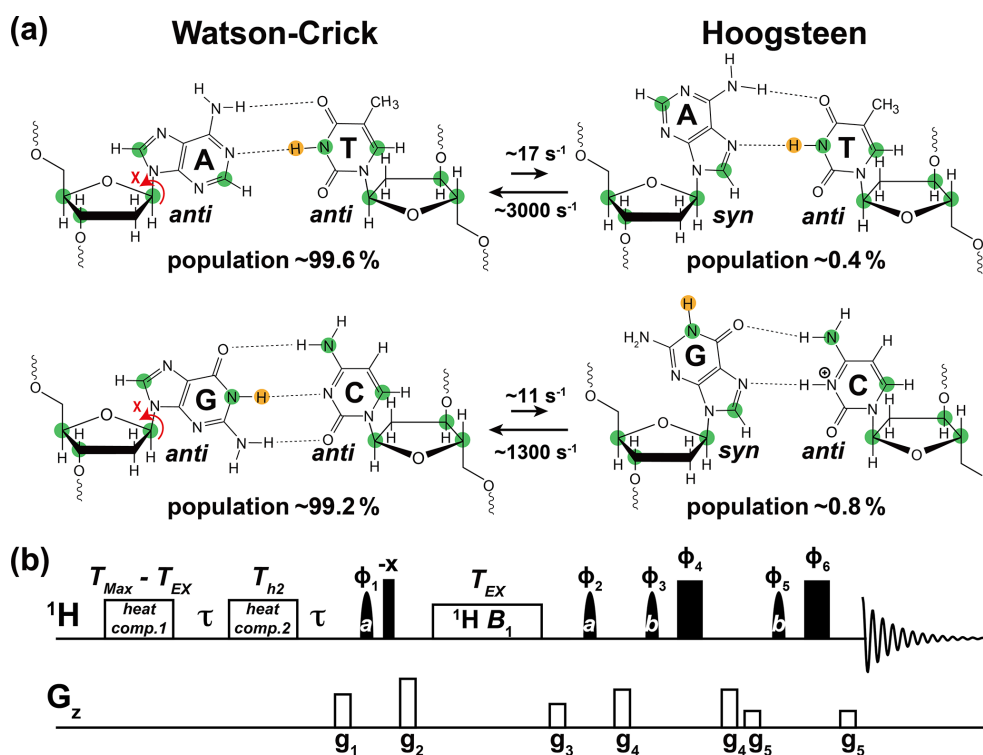


Figure 1. Using ^1H CEST to measure Watson–Crick to Hoogsteen exchange in unlabeled nucleic acid duplexes. **(a)** Watson–Crick G–C and A–T bp’s in B-DNA exist in dynamic equilibrium with G–C⁺ and A–T Hoogsteen bp’s, respectively. Filled green circles denote nuclei (^{13}C and ^{15}N) that have previously been used to probe the Watson–Crick to Hoogsteen exchange via RD measurements, while the yellow circle denotes the imino ^1H probes used in this study. Rate constants and populations were obtained as described previously (Alvey et al., 2014). **(b)** The 1D SELOPE ^1H CEST pulse sequence for characterizing chemical exchange in unlabeled nucleic acids. Narrow and wide filled rectangles denote 90 and 180° hard pulses. Semi-oval shapes denote selective pulses. Pulse a is a 90° Eburp2.1000 shape pulse (typically 3–4 ms) for selective excitation (excitation bandwidth ~ 2 –3 ppm) of imino protons, while pulse b is a 180° Squa100.1000 shape pulse with length 2 ms in an excitation sculpting scheme (Hwang and Shaka, 1995) for water suppression. Open rectangles denote the gradients and heat compensation elements. Delay $\tau = 1/2d_1 = 0.7\text{ s}$. To ensure uniform heating for experiments with variable lengths of T_{EX} , the relaxation period during which a ^1H B_1 field is applied, two heat compensation modules were used according to a prior study (Schlagnitweit et al., 2018). The first heat compensation is applied far off-resonance with duration = $T_{\text{Max}} - T_{\text{EX}} = 2\text{ ms}$, where T_{Max} is the maximum relaxation delay time. The second heat compensation (1 kHz) applied far off-resonance has a duration $T_{h2} = 150\text{ ms}$. The phase cycles used are $\phi_1 = \{8x, 8(-x)\}$, $\phi_2 = \{4x, 4(-x)\}$, $\phi_3 = \{x, y\}$, $\phi_4 = \{-x, -y\}$, $\phi_5 = \{2x, 2y\}$, and $\phi_6 = \{2(-x), 2(-y)\}$. Gradients (g₁–g₅) with SMSQ10.100 profiles are applied for 1 ms with the following amplitudes (G cm^{-1}): 14.445, 26.215, 14.445, 16.585, 5.885. The ^1H carrier is placed far offset (100 000 Hz) during the two heat compensation periods, then moved to the center of the imino resonances prior to the first pulse a. Next, the carrier is placed to a specified offset prior to the relaxation delay (T_{EX}), then placed back to the center of the imino resonances following T_{EX} . Finally, it is placed on-resonance with water for water suppression prior to pulse b. Briefly, imino ^1H magnetization is selectively excited, aligned longitudinally and then relaxes under a ^1H B_1 field during T_{EX} . ^1H transverse magnetization is then created and directly detected following water suppression. This pulse sequence is adapted from Schlagnitweit et al. (2018).

bp’s were shown to be lowly populated (population $< 1\%$) and short-lived (lifetime $\sim 1\text{ ms}$) forming robustly as an excited conformational state (ES) in duplex DNA across a variety of sequence contexts (Alvey et al., 2014) (Fig. 1a).

There is growing interest in mapping the Watson–Crick to Hoogsteen exchange landscape across different DNA contexts, including for bp’s in different sequence motifs (Alvey et al., 2014), near sites of damage and mismatches (Shi et al., 2021; Singh et al., 1993), and when DNA is bound to proteins (Nikolova et al., 2013b; Zhou et al., 2019) and drugs (Xu et al., 2018; Wang et al., 1984). Studies suggest an increased

propensity to form Hoogsteen bp’s in such environments (Shi et al., 2021), and this may in turn play a role in DNA recognition and damage repair (Afek et al., 2020). Furthermore, there is interest in understanding how the Hoogsteen exchange varies with temperature (Nikolova et al., 2011), pH (Nikolova et al., 2013a), salt concentration and buffer composition (Rangadurai et al., 2020b; Tateishi-Karimata et al., 2014), as well as in the presence of epigenetic modifications (Wang et al., 2017; Rangadurai et al., 2019a), all of which could shape these dynamics and consequently DNA biochemical transactions.

There are hundreds and thousands of motifs and conditions for which characterization of Hoogsteen dynamics is of biological interest. However, current approaches for measuring Hoogsteen dynamics are ill-suited for dynamics measurements at such a scale. The Watson–Crick to Hoogsteen chemical exchange process has been characterized with the use of ^{13}C (Nikolova et al., 2011; Shi et al., 2018; Ben Imed-dourene et al., 2020; Alvey et al., 2014) and ^{15}N (Nikolova et al., 2012a; Rangadurai et al., 2019a; Alvey et al., 2014) off-resonance $R_{1\rho}$, and more recently chemical exchange saturation transfer (CEST) experiments (Rangadurai et al., 2020b, a). However, these approaches require isotopically enriched DNA samples, making broad explorations of Hoogsteen exchange across even tens of motifs impractical. Furthermore, many motifs of interest involve damaged or modified nucleotides, which are difficult to isotopically enrich with ^{13}C and ^{15}N nuclei. It is therefore desirable to have more facile means to initially assess Watson–Crick to Hoogsteen exchange and to follow up with in-depth characterization for those motifs exhibiting interesting and unusual behavior. For such an initial screening application, we turned our attention to the imino ^1H as a probe of the Watson–Crick to Hoogsteen exchange in unlabeled DNA samples.

The utility of protons as probes in CEST (Chen et al., 2016; Dubini et al., 2020; Wang et al., 2021; Liu et al., 2021a), Carr–Purcell–Meiboom–Gill (CPMG) (Juen et al., 2016; LeBlanc et al., 2018), and off-resonance $R_{1\rho}$ experiments (Wang and Ikuta, 1989; Lane et al., 1993; Steiner et al., 2016; Schlagnitweit et al., 2018; Baronti et al., 2020; Furukawa et al., 2021) to study conformational exchange in nucleic acids is now well-established. Many of these ^1H -based approaches use experiments originally developed to study conformational exchange in proteins (Ishima et al., 1998; Eichmuller and Skrynnikov, 2005; Lundstrom and Akke, 2005; Lundstrom et al., 2009; Otten et al., 2010; Bouvignies and Kay, 2012; Hansen et al., 2012; Weininger et al., 2012, 2013; Smith et al., 2015; Sekhar et al., 2016; Yuwen et al., 2017a, b). The ^1H experiments permit the use of higher effective fields allowing characterization of conformational exchange faster than is possible using ^{13}C or ^{15}N experiments (Steiner et al., 2016; Palmer, 2014). Furthermore, the relationship between ^1H chemical shifts and structure is reasonably well understood and has been exploited in the conformational characterization of nucleic acids (Sripakdeevong et al., 2014; Frank et al., 2013; Wang et al., 2021; Swails et al., 2015; Czernek et al., 2000; Lam and Chi, 2010).

Recently, ^1H $R_{1\rho}$ and CEST SElective Optimized Proton Experiments (SELOPE) were developed and applied to characterize conformational exchange in unlabeled RNA (Schlagnitweit et al., 2018). The SELOPE experiment has already found several applications in studies of unlabeled nucleic acids, including in the characterization of fast ($k_{\text{ex}} = k_1 + k_{-1} > 1000 \text{ s}^{-1}$) RNA secondary structural rearrangements (Baronti et al., 2020) and DNA base opening (Furukawa et al., 2021), as well as slower ($k_{\text{ex}} < 100 \text{ s}^{-1}$) DNA

hybridization kinetics (Dubini et al., 2020). Many ^1H relaxation dispersion (RD) studies have targeted exchangeable imino protons (Baronti et al., 2020; Furukawa et al., 2021), taking advantage of the well-known dependence of the imino ^1H chemical shifts on secondary structure (Wang et al., 2021; Lam and Chi, 2010).

Although ^1H RD experiments can obviate the need for isotopic labeling and offer other advantages such as high sensitivity, they have not been as widely used compared to $^{13}\text{C}/^{15}\text{N}$ RD experiments. One reason for this has to do with potential artifacts arising due to from ^1H – ^1H cross-relaxation (Ishima et al., 1998; Eichmuller and Skrynnikov, 2005; Lundstrom and Akke, 2005; Bouvignies and Kay, 2012). Interestingly, in nucleic acids, such NOE effects appear to be effectively suppressed in the ^1H SELOPE experiment through selective excitation of spins (Schlagnitweit et al., 2018). The exchange parameters obtained using ^1H SELOPE experiments were shown to be in very good agreement with counterparts obtained using ^{13}C and ^{15}N off-resonance $R_{1\rho}$ (Baronti et al., 2020). In addition, similar exchange parameters were obtained when using variable tilt angles in $R_{1\rho}$ experiments, including tilt angle of 35.3° in which ROE and NOE cross-relaxation terms cancel (Eichmuller and Skrynnikov, 2005; Weininger et al., 2013; Steiner et al., 2016). No NOE dips or artifacts were observed in the majority of the ^1H CEST or off-resonance $R_{1\rho}$ profiles (Steiner et al., 2016; Dubini et al., 2020; Furukawa et al., 2021). These results are consistent with a prior off-resonance ^1H $R_{1\rho}$ studies showing that even without deuteration, it is feasible to effectively suppress cross-relaxation between amide and aliphatic protons through selective inversion of amide protons and use of short spin-lock relaxation delays (Lundstrom and Akke, 2005; Schlagnitweit et al., 2018). Nevertheless, NOE effects have been reported for select sites in ^1H SELOPE studies of nucleic acids (Schlagnitweit et al., 2018) and in ^1H CEST studies of proteins (Bouvignies and Kay, 2012; Sekhar et al., 2016; Yuwen et al., 2017a, b). This underscores the need to carefully analyze NOE effects, especially for unlabeled samples, in which spin-state-selective magnetization transfer schemes (Yuwen et al., 2017a, b) employing heteronuclei to suppress NOE effects are not feasible.

There are certain conditions in which the Hoogsteen bp becomes the dominant conformation in duplex DNA. These include chemically modified bases (Nikolova et al., 2011), when DNA is in complex with binding partners (Xu et al., 2018), and for specific sequence contexts under certain experimental conditions (Stelling et al., 2017). Based on NMR studies of such duplexes containing Hoogsteen bp's, there should be a sizable difference ($\Delta\omega \sim -1$ to -2 ppm) between the imino proton chemical shifts of guanine (G-H1) and thymine (T-H3) in the Hoogsteen versus Watson–Crick conformation. These differences should render G-H1 and T-H3 suitable probes of Hoogsteen exchange in unlabeled DNA duplexes provided that NOE effects can be effectively suppressed. Imino protons are also attractive probes given

that they are often well-resolved even in 1D ^1H spectra of large RNAs. Since no other ESs have been detected to date in several NMR studies of unmodified canonical DNA duplexes (Nikolova et al., 2011; Alvey et al., 2014; Shi et al., 2018; Ben Imeddourene et al., 2020), a single imino ^1H probe could be sufficient to reliably map and characterize the Watson–Crick to Hoogsteen exchange.

Here, we show that high-power ^1H CEST SELOPE experiments targeting the imino protons G-H1 and T-H3 provide facile means for initially assessing Watson–Crick to Hoogsteen exchange of G–C and A–T bp's in DNA without the need for isotopic enrichment. NOE effects are shown to have a negligible contribution as short (≤ 100 ms) relaxation delays can be used to characterize the relatively fast ($k_{\text{ex}} \sim 500$ to 8000 s^{-1}) Watson–Crick to Hoogsteen exchange process (Alvey et al., 2014). The approach also takes advantage of high-power radio-frequency (RF) fields recently shown (Rangadurai et al., 2020a) to extend the timescale sensitivity of CEST to include faster exchange processes that traditionally are more effectively characterized with the use of $R_{1\rho}$. The high-power ^1H CEST experiment also enabled measurement of fast Hoogsteen exchange kinetics ($k_{\text{ex}} > 20\,000\text{ s}^{-1}$) inaccessible to conventional ^{13}C or ^{15}N off-resonance $R_{1\rho}$ RD. The ^1H CEST experiment opens the door to more comprehensively and systematically exploring how the Watson–Crick to Hoogsteen exchange process varies with sequence and structural contexts and physiological conditions of interest.

2 Results

2.1 Assessment of NOE effects

We used the SELOPE (Schlagnitweit et al., 2018) experiment (Fig. 1b) to measure ^1H CEST profiles for G-H1 and T-H3 in unlabeled DNA duplexes (Fig. 2) at 25–26 °C. We used ^1H CEST rather than $R_{1\rho}$ given the greater ease of collecting profiles for many spins simultaneously, and given that with the use of high-power RF fields, CEST can effectively characterize exchange processes over a wide range of timescales (Rangadurai et al., 2020a). Use of high-power RF fields was recently shown to be important to effectively characterize the comparatively fast ($k_{\text{ex}} \sim 3000\text{ s}^{-1}$) Watson–Crick to Hoogsteen exchange process using ^{13}C and ^{15}N CEST experiments (Rangadurai et al., 2020a). Here, we also employed high-power RF fields ($> 250\text{ Hz}$) to optimally characterize Watson–Crick to Hoogsteen exchange using ^1H CEST.

An important consideration when performing ^1H CEST experiments is contributions due to ^1H – ^1H cross-relaxation, which may give rise to extraneous NOE dips in the ^1H CEST profiles (Ishima et al., 1998; Lundstrom and Akke, 2005; Eichmuller and Skrynnikov, 2005; Bouvignies and Kay, 2012; Sekhar et al., 2016; Yuwen et al., 2017a, b). These contributions have been suppressed in proteins through deuteration (Eichmuller and Skrynnikov, 2005; Lundstrom and

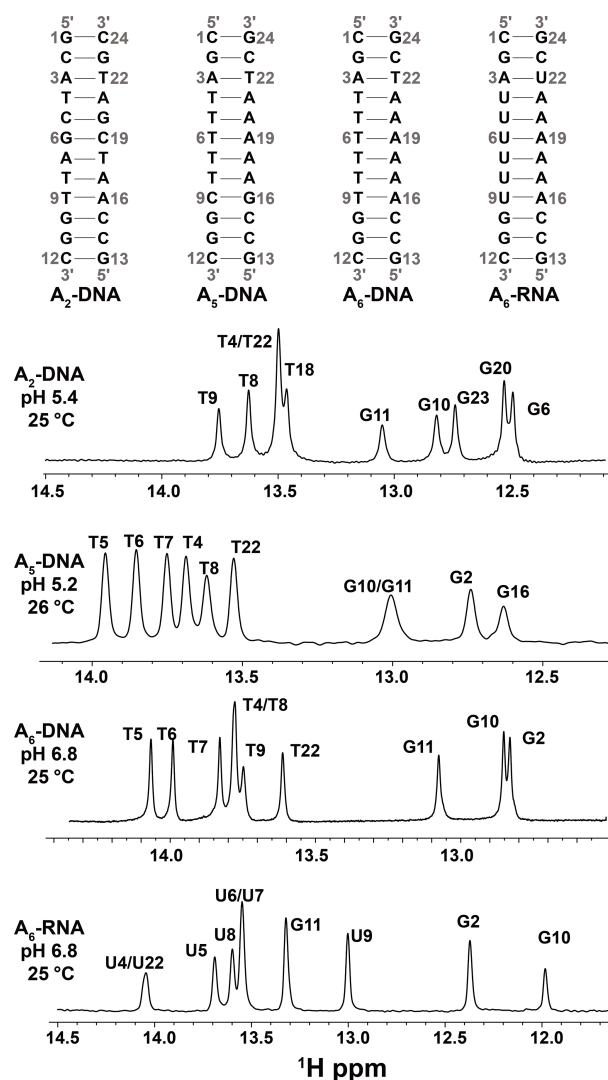


Figure 2. DNA and RNA duplexes used in this study. Also shown are 1D ^1H spectra of the imino region. The buffer conditions were 25 mM sodium chloride, 15 mM sodium phosphate, 0.1 mM EDTA and 10 % D_2O . The pH and temperature are indicated on each spectrum.

Akke, 2005; Lundstrom et al., 2009; Otten et al., 2010; Hansen et al., 2012; Weininger et al., 2012), in ^{15}N isotopically labeled proteins (Yuwen et al., 2017a, b) and nucleic acids (Wang et al., 2021; Liu et al., 2021a) using spin-state-selective magnetization transfer schemes, and through selective inversion of protons combined with use of short relaxation times (Lundstrom and Akke, 2005; Schlagnitweit et al., 2018).

In the SELOPE experiment, imino protons are selectively excited, and the magnetization belonging to non-imino protons is dephased prior to application of the B_1 field. This helps to suppress cross-relaxation (Yamazaki et al., 1994) between the imino and non-imino protons (vide infra). In addition, because the Watson–Crick to Hoogsteen exchange is

relatively fast with $k_{\text{ex}} = \sim 500\text{--}8000\text{ s}^{-1}$ at $25\text{ }^\circ\text{C}$ (Alvey et al., 2014), we could afford to use a relatively short relaxation delay of 100 ms, which also helped minimize NOE effects (vide infra) (Lundstrom and Akke, 2005; Schlagnitweit et al., 2018).

We initially performed experiments to evaluate contributions from $^1\text{H}\text{--}^1\text{H}$ cross-relaxation to the imino ^1H CEST profiles. In canonical B-form DNA and A-form RNA duplexes (Fig. 2), G-H1 is in closest proximity to the partner base C-H4a ($\sim 2.4\text{ \AA}$, Fig. 3a), while T/U-H3 is in closest proximity to the partner A-H2 ($\sim 2.8\text{ \AA}$, Fig. 3a). Additional proximal protons include imino and H2 protons of neighboring residues ($\sim 3.5\text{--}3.6\text{ \AA}$, Fig. 3a). These short internuclear distances are reflected in the intensity of cross peaks in 2D [^1H , ^1H] NOESY spectra of nucleic acid duplexes (Figs. 3b and S1 in the Supplement). Note that although the amino proton of G-H2a is in proximity (2.2 \AA) to G-H1, while the amino proton of A-H6a is in proximity (2.4 \AA) to the partner T-H3 (Fig. 3a), these amino protons are typically not observable in 1D ^1H or 2D [^1H , ^1H] NOESY spectra caused by intermediate exchange due to the restricted rotation around the C–NH₂ bond (Schnieders et al., 2019).

^1H CEST profiles (Figs. 3b and S2) for well-resolved imino resonances of A₆-DNA (Fig. 2) were acquired simultaneously in a 1D manner using $\sim 3\text{ h}$ of acquisition time on a spectrometer operating at 600 MHz ^1H frequency equipped with a cryogenic probe, using $\sim 1.0\text{ mM}$ unlabeled DNA (Methods). Data were initially collected at pH = 6.8. Under these near-neutral pH conditions, it is generally not feasible to detect the Watson–Crick to Hoogsteen exchange process for G–C bp's due to the low population of the protonated G–C⁺ Hoogsteen bp's (Nikolova et al., 2013a). The lack of expected dips for the ES G–C⁺ Hoogsteen bp's under these conditions provides an opportunity to better assess any extraneous ^1H CEST dips arising due to NOE effects. Unlike for G–C bp's, the Hoogsteen exchange should still be detectable for A–T bp's under these pH conditions.

Shown in Fig. 3b is a representative imino ^1H CEST profile measured for G2-H1 in the well-characterized A₆-DNA duplex (Nikolova et al., 2011). Besides the major dip, no additional dips were visible in the ^1H CEST profile. The major dip was also symmetric (Rangadurai et al., 2020a), indicating little to no contribution from Hoogsteen exchange or NOE effects, as expected for G–C bp's under these pH conditions (Nikolova et al., 2013a). On the other hand, a minor shoulder was observed in the ^1H CEST profile of T5-H3 (Fig. 3b, the $\Delta\omega$ is highlighted by a dashed red line and labeled “ES”). The shoulder occurs at an offset frequency that does not correspond with any other observable proton frequency in the A₆-DNA duplex and is therefore unlikely to be the result of NOE effects (Fig. 3a). Rather, as will be described below, the shoulder corresponds to the ES Hoogsteen bp, which is to be expected for the A–T bp at pH = 6.8.

To further verify that the dips observed in the ^1H CEST profile of T5-H3 and other thymine residues in A₆-DNA (see

Figs. 4 and S2) do not represent an NOE effect, but rather reflect the ES Hoogsteen bp, we performed ^1H CEST experiments on a corresponding A₆-RNA duplex (Fig. 2). Unlike in B-form DNA duplexes, G–C⁺ and A–U Hoogsteen bp's are both undetectable in A-form RNA duplexes by off-resonance ^{13}C and ^{15}N $R_{1\rho}$ RD, most likely due their much lower population ($p_{\text{ES}} < 0.04\%$) (Zhou et al., 2016; Rangadurai et al., 2018). If the shoulder observed in the ^1H CEST profile of T5-H3 in A₆-DNA is due to a Hoogsteen ES, and not NOE dips, we would expect to observe a symmetric profile without ES dips for U5-H3 in A₆-RNA. Indeed, the corresponding ^1H CEST profiles for U5-H3 (Fig. 4) and all other uridine and guanine (Fig. S3) imino protons in A₆-RNA were symmetric, with no evidence for any asymmetry or shoulder, indicating the absence of exchange and NOE effects.

Therefore, the shoulders in the ^1H CEST profiles (Figs. 3, 4, S2, S3) most likely rise due to chemical exchange with an ES. This was further confirmed by evaluating whether fits to the ^1H CEST profiles show any statistically significant improvement with the inclusion of exchange, as described below. Based on a similar analysis, no NOE dips were observable in the ^1H CEST profiles (Figs. 4, S2, S3) for all other residues in A₆-DNA, A₆-RNA, and in two other DNA duplexes across a range of pH and temperature conditions when using selective excitation and relaxation delay of 100 ms (Figs. 2, 4, S2, S3). These results indicate that any NOE effects between imino and non-imino protons are small under these experimental conditions.

Upon increasing the relaxation delay to 400 ms or using a non-selective ^1H excitation pulse (pulse a in Fig. 1b) with a delay of 100 ms, NOE dips became visible in the ^1H CEST profiles as shown for G2-H1 and T5-H3 (Fig. 3b) in A₆-DNA. The dips occurred at the ^1H resonance frequency of nearby protons and, as expected, were particularly pronounced for the partner C-H4a in the case of G2-H1 and the partner A-H2 in the case of T5-H3 (Fig. 3b). Nevertheless, even the ^1H CEST profiles acquired with 400 ms delay could be fit when restricting the offset to the imino proton region (-3 to 3 ppm), and the fitted exchange parameters were similar to those obtained from fitting profiles with 100 ms relaxation delay in which no NOE dips were visible (Fig. S4, Table S1). In contrast, the ^1H CEST profiles measured using non-selective excitation, which had larger NOE dips relative to using a selective excitation pulse, could not be satisfactorily fit (Fig. S4).

No NOE dips were observed at the chemical shift of imino protons belonging to neighboring residues in ^1H CEST profiles measured in DNA and RNA duplexes, and none of the ^1H CEST profiles collected in this study yielded an ES with $\Delta\omega$ compatible with the imino ^1H chemical shift of a neighboring residue. Nevertheless, these NOE effects could be more difficult to assess given that they would be buried within the major dip. While imino–imino ^1H NOEs are not suppressed by selective excitation, their contribution is expected to be smaller relative to other NOE

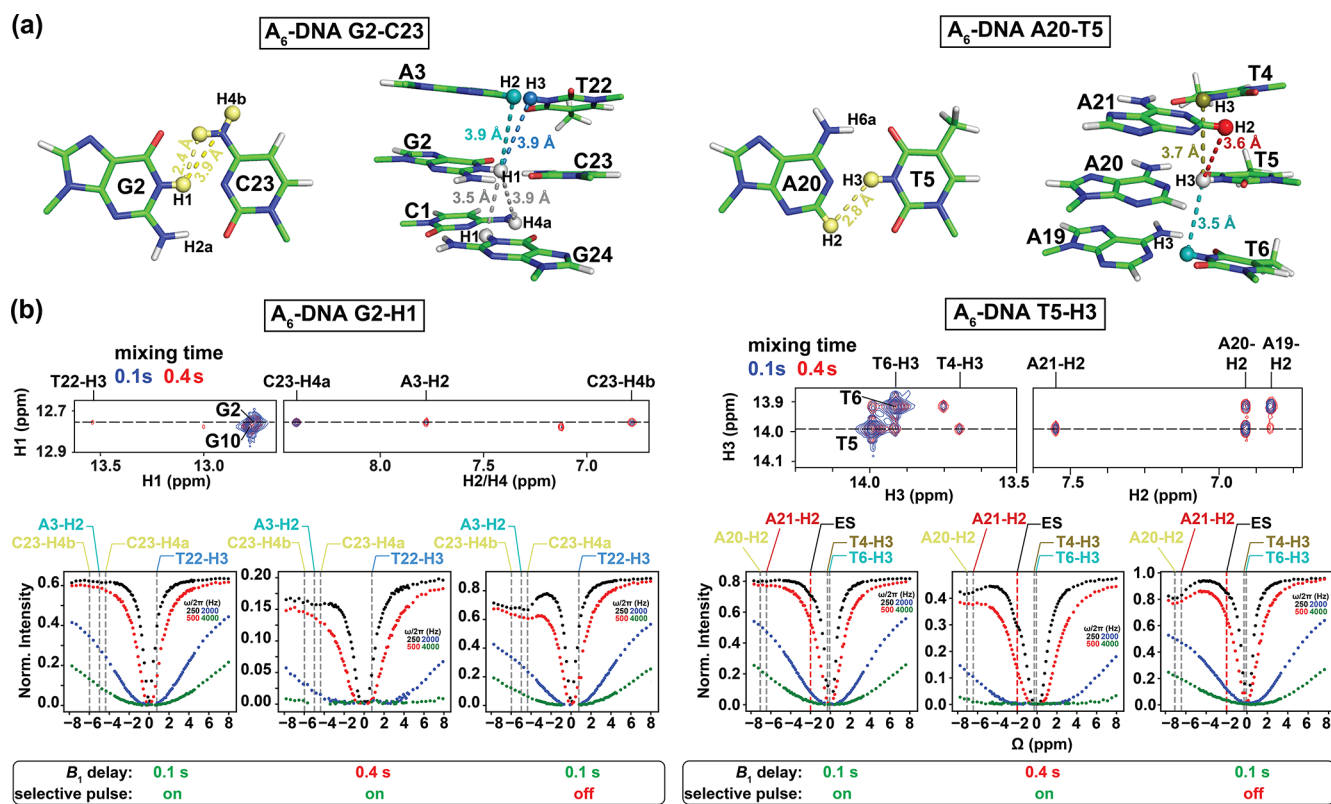


Figure 3. Analysis of NOE effects in ^1H CEST profiles. (a) Distances between the imino protons of G2-H1 and T5-H3 and nearby protons in the A₆-DNA duplex (PDBID: 5UZF). Note that although the amino proton of G-H2a is in proximity (2.2 Å) to G-H1, while the amino proton of A-H6a is in proximity (2.4 Å) to the partner T-H3, these amino protons are not observable in 1D ^1H or 2D [^1H , ^1H] NOESY spectra caused by intermediate exchange due to the restricted rotation around the C–NH₂ bond (Schnieders et al., 2019). (b) NOE dips in ^1H CEST profiles for G2-H1 and T5-H3 in A₆-DNA. The NOE diagonal and cross peaks for G2-H and T5-H3 in the 2D [^1H , ^1H] NOESY spectra with mixing time 100 ms (blue) and 400 ms (red) are shown on the top. The ^1H CEST profiles for G2-H1 and T5-H3 with combinations of short (100 ms) and long (400 ms) relaxation delays, with and without selective excitation (Methods), are shown at the bottom. The ES frequency (black) obtained from fitting ^1H CEST profiles with selective excitation and short relaxation delay (100 ms) as well as frequency positions corresponding to the NOE cross peaks in the 2D [^1H , ^1H] NOESY spectra (top) are highlighted according to the color scheme in (a) (bottom). Error bars for CEST profiles in (b), which are smaller than the data points, were obtained using triplicate experiments, as described in Methods. RF powers for CEST profiles are color-coded.

dips observed when using non-selective excitation (distances ~ 2.4 – 2.8 Å between guanine/thymine imino and cytosine amino/adenine H2) due the larger distance of separation between neighboring imino protons (~ 3.5 – 3.9 Å) (Fig. 3a).

To further assess the impact of imino–imino ^1H NOEs on the ^1H CEST profiles, we examined whether selective excitation of imino protons (but not their immediate neighbors) results in different ^1H CEST profiles relative to an experiment in which all imino protons are excited. We performed an experiment selectively exciting G10-H1 and G2-H1 in A₆-DNA without exciting the imino resonances belonging to either of their two immediate neighbors. Selective excitation of individual imino protons resulted in ^1H CEST profiles (Fig. S2) and fitted parameters (Table S1) for G10-H1 and G2-H1 that are within error to those obtained when exciting all imino protons, again indicating that any imino–imino NOE contribution is negligible. Finally, the impact of imino–

imino NOEs on the determination of the exchange parameters was also assessed (vide infra) through comparison of the exchange parameters derived from fitting the imino ^1H CEST profiles with those measured independently using off-resonance ^{13}C and ^{15}N $R_{1\rho}$ RD measurements.

These results underscore the importance of critically evaluating the NOE contributions on a case-by-case basis (Schlagintweit et al., 2018) and also suggest that NOE effects can be effectively suppressed for the canonical duplexes used in this study provided use of selective excitation and short relaxation delays.

It should be noted that to avoid any complexities due to NOE effects with water protons or hydrogen exchange, we restricted the offset to -6 to 6 ppm when analyzing and fitting the ^1H CEST profiles. This is common practice as relatively narrow offsets (< 4 ppm) were used in prior ^1H CEST studies of both nucleic acids (Dubini et al., 2020; Wang et al.,

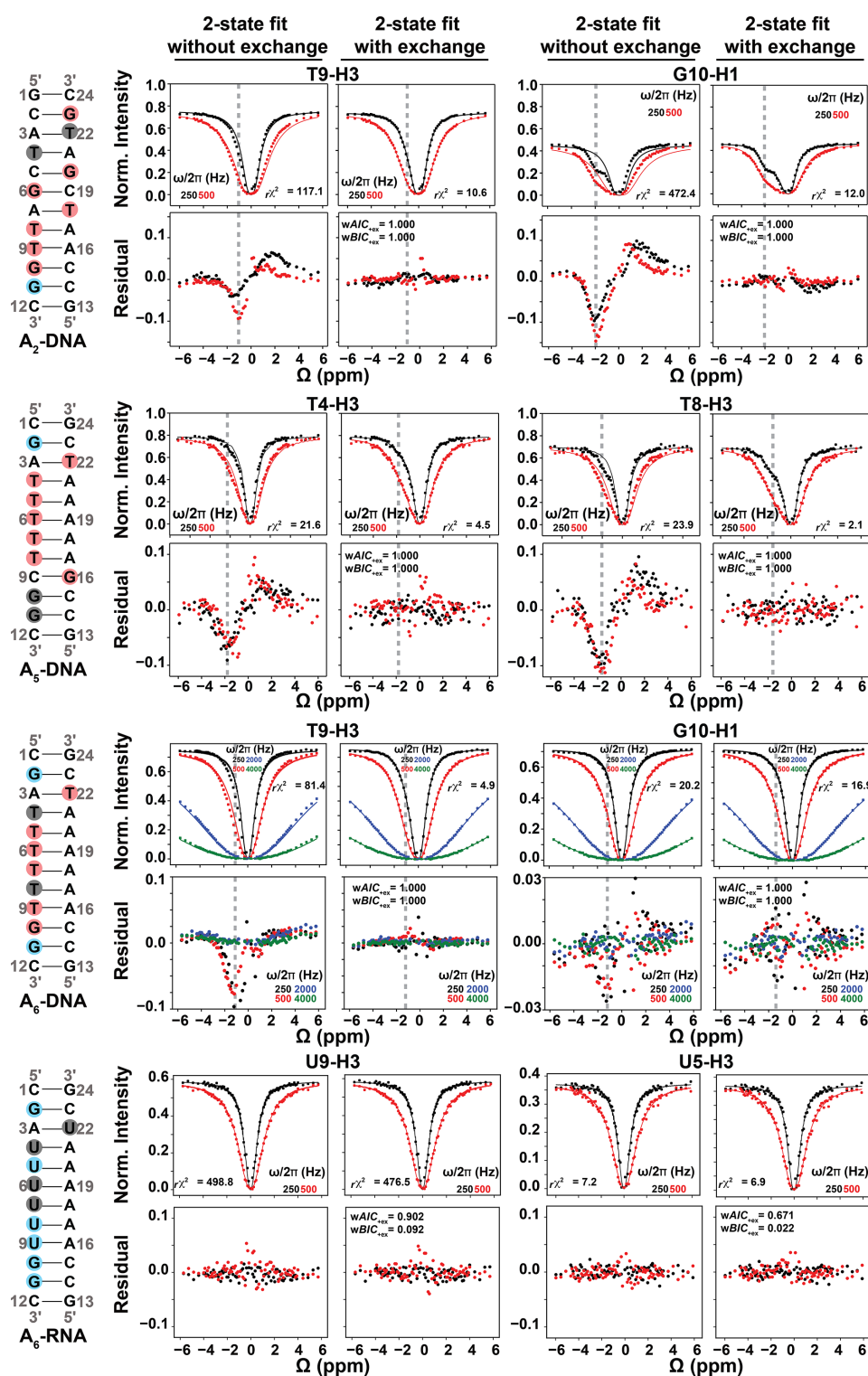


Figure 4. Representative ^1H CEST profiles measured for A_2 -DNA (pH 5.4) at 25°C , A_5 -DNA (pH 5.2) at 26°C , A_6 -DNA (pH 6.8) at 25°C and A_6 -RNA (pH 6.8) at 25°C . Residues with detectable RD, undetectable RD and overlapped 1D ^1H resonances (see Fig. 2) are highlighted in red, blue and gray circles respectively. Shown are the fits of the ^1H CEST data to a two-state Bloch–McConnell equation with and without ($k_{\text{ex}} = \Delta\omega = p_{\text{ES}} = 0$) chemical exchange. Shown below the CEST profiles are residual (experimental normalized intensity – fitted normalized intensity) plots. Also shown are the reduced chi-square (r^2), and Akaike's (wAIC) and Bayesian information criterion (wBIC) weights for fits with exchange (Methods). The dashed gray lines indicate the Hoogsteen $\Delta\omega$ positions in both ^1H CEST profiles and in residual plots. Error bars for CEST profiles, which are smaller than the data points, were obtained using triplicate experiments, as described in Methods. RF powers for CEST profiles are color-coded.

2021; Liu et al., 2021a) and proteins (Yuwen et al., 2017a, b). While we did not observe a dip near the water chemical shift in the ^1H CEST profile for the internal residue T5-H3, a weak and broad dip near the water chemical shift was observed in the profile for the near-terminal residue G2-H1 (Fig. S2). The latter dip could be due to NOEs between G2-H1 and water protons and/or due to fast hydrogen exchange kinetics.

2.2 Benchmarking the utility of ^1H CEST to probe Watson–Crick to Hoogsteen exchange in DNA duplexes

To examine the utility of the SELOPE ^1H CEST experiment to characterize Watson–Crick to Hoogsteen exchange, we benchmarked the experiment by measuring conformational exchange in three DNA duplexes (A_6 -DNA, A_2 -DNA and A_5 -DNA, Fig. 2) for which we have previously extensively characterized the Watson–Crick to Hoogsteen exchange using ^{13}C and ^{15}N off-resonance $R_{1\rho}$ (Nikolova et al., 2011; Alvey et al., 2014; Shi et al., 2018) and CEST (Rangadurai et al., 2020a, b) experiments. We compared the exchange parameters derived using ^1H CEST with counterparts derived using $^{13}\text{C}/^{15}\text{N}$ $R_{1\rho}$ or CEST for a variety of G–C and A–T bp's across three different DNA duplexes and varying pH (5.2–6.8) conditions. All ^1H CEST experiments were performed using 100 ms relaxation delay and selective excitation.

As expected, for several thymine residues, the imino ^1H CEST profile was visibly asymmetric (Figs. 4, S2, S3), consistent with relatively fast ($k_{\text{ex}} > 1000 \text{ s}^{-1}$) Watson–Crick to Hoogsteen exchange. The asymmetry manifests as an upfield shifted shoulder (e.g., T8-H3 in A_5 -DNA in Fig. 4) as expected for T-H3 Hoogsteen chemical shift ($\Delta\omega \sim -2$ ppm) (Nikolova et al., 2011; Xu et al., 2018). In other cases, such as T9-H3 in A_6 -DNA, the asymmetry was less pronounced, and the exchange contribution was only apparent following comparison of fits with and without exchange (see Fig. 4).

As expected, at pH = 6.8, the imino ^1H CEST profiles were symmetric for most guanine residues consistent with no observable exchange (Figs. 4, S2, S3). However, the major dip became asymmetric for several guanine residues when lowering the pH to 5.2 or 5.4, as expected for the Watson–Crick to Hoogsteen exchange of G–C bp's, which is favored at lower pH (Figs. 4 and S3). All minor dips occurred at resonance frequencies that did not correspond with any other protons in the molecule (Figs. 2, S1, S2). In all cases, the ^1H CEST profiles could be satisfactorily fit to a two-state model with or without exchange, suggesting that any NOE contribution to the ^1H CEST profile is likely to be insignificant.

To identify which imino ^1H CEST profiles have significant chemical exchange contributions, each profile was subjected to a fit with or without ($\Delta\omega = p_{\text{ES}} = k_{\text{ex}} = 0$) two-state chemical exchange (Methods). Akaike information criterion (AIC) and Bayesian information criterion (BIC) (Burnham and Anderson, 2004) weights were then used to evaluate

whether any improvement in the fit due to inclusion of chemical exchange was statistically significant (Kimsey et al., 2018; Liu et al., 2021a). The improvement of fit was considered to be statistically significant when both AIC and BIC weights are > 0.995 and the reduced chi-square ($r\chi^2$) is reduced with the inclusion of exchange. Residual plots were also used to visualize changes in fit quality (Fig. 4).

Based on the AIC and BIC analysis, all thymine and guanine residues shown previously to undergo Watson–Crick to Hoogsteen exchange using off-resonance ^{13}C and/or ^{15}N $R_{1\rho}$ under these experimental conditions also showed statistically significant improvements when fitting the ^1H CEST profiles with the inclusion of chemical exchange (Figs. 4, S2, S3). On the other hand, all guanine residues, including G2 and G11 in A_6 -DNA and G11 in A_2 -DNA, which did not show signs of Hoogsteen exchange in off-resonance ^{13}C and/or ^{15}N $R_{1\rho}$ (Nikolova et al., 2011; Shi et al., 2018) under these experimental conditions, also did not show statistically significant improvements when fitting their ^1H CEST profiles with the inclusion of chemical exchange (Figs. 4, S2, S3).

Interestingly, a few residues, including T5, T6, T7 and T22 in A_6 -DNA and T18, G6 and G20 in A_2 -DNA (Figs. S2, S3), showed exchange based on ^1H CEST but did not show evidence for Hoogsteen exchange based on prior off-resonance ^{13}C and/or ^{15}N $R_{1\rho}$ experiments (Nikolova et al., 2011; Alvey et al., 2014; Shi et al., 2018). As will be elaborated in the following section, these data provide new insights into the Watson–Crick to Hoogsteen exchange process and suggest that at least in some cases, ^1H CEST can exceed the detection limits of $^{13}\text{C}/^{15}\text{N}$ -based methods.

In addition, T18 and G20 in A_2 -DNA were difficult to probe using ^{13}C RD due to spectra overlap (Nikolova et al., 2011) but could easily be measured using ^1H CEST (Figs. 2, 4 and S3). In contrast, other residues such as T8 and T4 in A_6 -DNA, T4 and T22 in A_2 -DNA, and G10 and G11 in A_5 -DNA could be targeted for ^{13}C or ^{15}N RD measurements (Nikolova et al., 2011; Alvey et al., 2014) but could not be measured by ^1H CEST due to overlap in the 1D ^1H imino spectra (Fig. 2). This highlights the complementarity of ^1H and $^{13}\text{C}/^{15}\text{N}$ RD in characterizing Watson–Crick to Hoogsteen exchange.

To assess how well the exchange parameters are determined by the ^1H CEST data, we subjected the ^1H CEST profiles for residues T7 ($k_{\text{ex}}/\Delta\omega \sim 0.2$), T9 ($k_{\text{ex}}/\Delta\omega \sim 0.82$) and T22 ($k_{\text{ex}}/\Delta\omega \sim 3.5$), which exhibit exchange on the slow, intermediate and fast timescales (Rangadurai et al., 2019b) respectively, to a degeneracy analysis. We computed the reduced chi-square ($r\chi^2$) for a two-state fit as a function of varying k_{ex} , $\Delta\omega$ or p_{ES} . In all cases, the $r\chi^2$ values increased significantly (up to 10-fold) when varying k_{ex} , $\Delta\omega$ or p_{ES} by 3-fold (Fig. S5), indicating that the exchange parameters are well-defined by the ^1H CEST data.

To test the accuracy of the exchange parameters obtained using ^1H CEST, we compared the exchange parameters p_{ES} and k_{ex} , derived from a two-state fit of the data to values de-

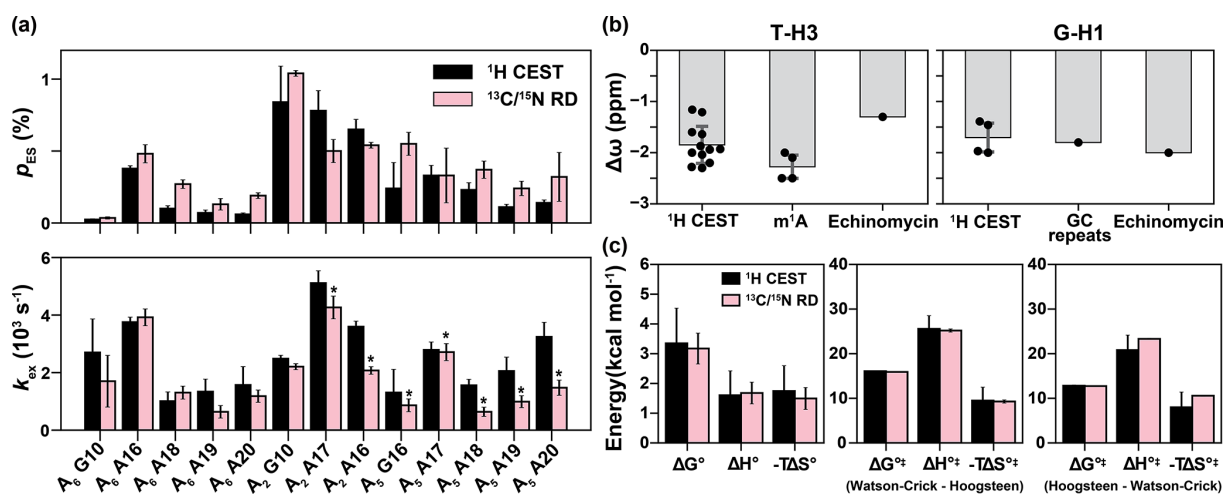


Figure 5. Comparison of exchange parameters for the Watson–Crick to Hoogsteen exchange obtained from ^1H CEST and $^{13}\text{C}/^{15}\text{N}$ $R_{1\rho}$. (a) Comparison of exchange parameters (k_{ex} and p_{ES}) measured using ^1H CEST with counterparts previously reported using $^{13}\text{C}/^{15}\text{N}$ off-resonance $R_{1\rho}$ (Nikolova et al., 2011; Alvey et al., 2014; Shi et al., 2018). ^{13}C RD data for A18, A19 and A20 were measured using off-resonance $R_{1\rho}$ in this study (Fig. S7). Small systematic deviations in k_{ex} for the values indicated with asterisks could be due to small differences in temperature ($< 0.8^\circ\text{C}$) across different spectrometers. The bp's are specified by the corresponding purine residue. (b) Comparison of the $\Delta\omega$ obtained from fitting ^1H CEST profiles for T-H3 and G-H1 (Table S1) with the values expected for a Watson–Crick to Hoogsteen transition based on duplexes in which A–T or G–C⁺ Hoogsteen bp's were rendered the dominant state, by using *N*¹-methylated adenine (m¹A) (Nikolova et al., 2011; Sathyamoorthy et al., 2017; Rangadurai et al., 2020b), by binding of the drug (echinomycin) to a DNA duplex (Xu et al., 2018), or through use of GC repeat sequences (GC repeats) that predominantly form Hoogsteen bp's at low pH (Stelling et al., 2017). (c) Comparison of free energy (ΔG°), enthalpy (ΔH°) and entropy ($-T\Delta S^\circ$, $T = 25^\circ\text{C}$) of the Watson–Crick to Hoogsteen transition, and the activation free energy (ΔG^{\ddagger}), enthalpy (ΔH^{\ddagger}) and entropy ($-T\Delta S^{\ddagger}$, $T = 25^\circ\text{C}$) for Watson–Crick to Hoogsteen (Watson–Crick–Hoogsteen) and Hoogsteen to Watson–Crick (Hoogsteen–Watson–Crick) transitions measured using ^1H CEST in this study and using ^{13}C $R_{1\rho}$ from Nikolova et al. (2011). The energetics in (c) were measured for the Watson–Crick to Hoogsteen transition of A16–T9 in A₆-DNA at pH 6.8. Errors in (a) were fitting errors of ^1H CEST, calculated as described in Methods or errors of $^{13}\text{C}/^{15}\text{N}$ $R_{1\rho}$ calculated using a Monte Carlo scheme as described previously (Rangadurai et al., 2019b). Errors in (b) are the standard deviations of data points (shown as black dots) in each category. Error bars in (c) were propagated from the errors in the exchange parameters obtained from ^1H CEST or $^{13}\text{C}/^{15}\text{N}$ $R_{1\rho}$.

terminated previously using off-resonance ^{13}C and/or ^{15}N $R_{1\rho}$ (Nikolova et al., 2011; Shi et al., 2018; Alvey et al., 2014) for Hoogsteen dynamics (Fig. 5a and Table S1). In total, we were able to compare 13 data points from ^1H CEST and $^{13}\text{C}/^{15}\text{N}$ $R_{1\rho}$ for three different duplexes under different conditions of temperature and pH (Figs. 2, 5a). This comparison also allowed us to further verify that the exchange process detected by ^1H CEST does indeed correspond to Watson–Crick to Hoogsteen exchange and to also further assess for potential contributions from NOE effects, which might cause deviations from agreement.

Indeed, the p_{ES} and k_{ex} values derived using ^1H CEST were in very good agreement with their off-resonance ^{13}C and/or ^{15}N $R_{1\rho}$ counterparts (Fig. 5a). The differences between k_{ex} and p_{ES} measured using the two methods were often within error with the largest differences being < 3 -fold. A small and systematic difference in k_{ex} was observed for a subset of the data (Fig. 5a), and this might be due to small temperature differences ($< 0.8^\circ\text{C}$) between spectrometers. Importantly, the ES imino ^1H chemical shifts deduced from a two-state fit of the ^1H CEST profiles ($\Delta\omega_{\text{A-T}} \approx -1$

to -2 ppm and $\Delta\omega_{\text{G-C}} \approx -1.5$ to -2.0 ppm) were also in good agreement with the expected range of values ($\Delta\omega = -1$ to -2 ppm) for Hoogsteen bp's (Fig. 5b) based on studies of duplexes containing Hoogsteen bp's as the dominant conformation (Nikolova et al., 2011; Stelling et al., 2017; Xu et al., 2018; Rangadurai et al., 2020b).

As an additional test, we also measured temperature-dependent (5, 10, 20, 25, 30 and 45°C) ^1H CEST profiles for A₆-DNA at pH 6.8 (Fig. S2) and then used the temperature dependence of the fitted kinetic rate constants (k_1 and k_{-1}) to determine the standard and activation enthalpy and entropy changes for the Watson–Crick to Hoogsteen transition (Fig. S6). These values were in excellent agreement with those measured from off-resonance ^{13}C $R_{1\rho}$ (Nikolova et al., 2011) (Fig. 5c), further supporting the robustness of the ^1H CEST methodology.

2.3 New insights into Hoogsteen breathing

^1H CEST profiles for some residues show detectable exchange contributions when corresponding $^{13}\text{C}/^{15}\text{N}$ RD

measurements do not or show only weak exchange. This suggests that ^1H CEST can provide additional insights into Watson–Crick to Hoogsteen exchange and extend the detection limits of conventional $^{13}\text{C}/^{15}\text{N}$ RD measurements.

For example, using ^1H CEST it was feasible to measure Watson–Crick to Hoogsteen exchange for T5-H3, T6-H3 and T7-H3 (Fig. S2) within the middle of the A-tract motif (defined as A_n -tract with $n > 3$) in A_6 -DNA. These residues had previously exhibited only weak on-resonance ^{13}C $R_{1\rho}$ RD, and as a result, no off-resonance $R_{1\rho}$ data were ever recorded (Nikolova et al., 2011). Based on the ^1H CEST measurements, residues within the A-tract motif have 10-fold lower Hoogsteen population ($p_{\text{ES}} = 0.06 \pm 0.01\% - 0.09 \pm 0.03\%$) relative to other A–T bp's in A_6 -DNA ($p_{\text{ES}} > \sim 0.10\%$) (Table S1). These represent the lowest A–T Hoogsteen populations ever recorded to date in duplex DNA (Table S1). The exchange kinetics were also 2-fold slower ($k_{\text{ex}} \sim 1000 \text{ s}^{-1}$) for the A-tract residues relative to other A–T bp's ($k_{\text{ex}} > 2000 \text{ s}^{-1}$) in A_6 -DNA (Table S1). Interestingly, the suppression of Hoogsteen dynamics within the A-tract motif appears to be A-tract length dependent, with both the Hoogsteen population and exchange kinetics increasing slightly for similar bp's in A_5 -DNA (Table S1). The suppression of Hoogsteen dynamics within A-tracts is consistent with prior studies showing them to be more rigid and stiff motifs relative to scrambled DNA (Nikolova et al., 2012b). We verified these ^1H CEST-derived exchange parameters for A-tract residues in A_6 -DNA by performing off-resonance ^{13}C $R_{1\rho}$ measurements (Fig. S7) on uniformly $^{13}\text{C}/^{15}\text{N}$ -labeled A_6 -DNA and did indeed observe the expected RD with p_{ES} and k_{ex} values similar (difference < 3 -fold, Fig. 5a) to those measured using ^1H CEST. These prospective tests of the ^1H CEST data using off-resonance $^{13}\text{C}/^{15}\text{N}$ $R_{1\rho}$ RD data further support the methodology.

The ability to characterize fast exchange kinetics has long been a motivation for using ^1H in RD experiments to characterize conformational exchange (Ishima et al., 1998; Ishima and Torchia, 2003; Eichmuller and Skrynnikov, 2005; Lundstrom and Akke, 2005; Otten et al., 2010; Hansen et al., 2012; Smith et al., 2015; Steiner et al., 2016; Furukawa et al., 2021). Indeed, ^1H CEST made it possible to measure fast Watson–Crick to Hoogsteen exchange kinetics which were undetectable by off-resonance ^{13}C $R_{1\rho}$. In particular, it was possible to measure Watson–Crick to Hoogsteen exchange for T22 in A_6 -DNA with $k_{\text{ex}} > 20\,000 \text{ s}^{-1}$ (Fig. S2 and Table S1), which is the fastest ever recorded Hoogsteen exchange process at 25°C (Table S1). In contrast, the off-resonance ^{13}C $R_{1\rho}$ RD profiles reported for this residue in prior studies were flat (Nikolova et al., 2011; Shi et al., 2018), and simulations show that such an exchange process is too fast for reliable detection using ^{13}C $R_{1\rho}$ (Fig. S8a). Similarly, it was feasible to measure Watson–Crick to Hoogsteen exchange for G6 ($p_{\text{ES}} \sim 0.3\%$, $k_{\text{ex}} \sim 3000 \text{ s}^{-1}$) in A_2 -DNA using ^1H CEST, yet no off-resonance ^{13}C $R_{1\rho}$ RD on C1' was previously detected (Shi et al., 2018), which based on simu-

lations, was likely due to a combination of exchange kinetics and small $\Delta\omega$ value (Fig. S8b).

One of the potential utilities of the ^1H CEST experiment is the measurement of very fast exchange kinetics at high temperatures and in a manner insensitive to melting of duplexes, shown previously to complicate analysis of Hoogsteen exchange using ^{13}C and ^{15}N RD (Shi et al., 2019). Melting of duplexes should not yield any exchange dips around the imino ^1H region given that the imino protons of single-stranded species (ssDNA) exchange rapidly with solvent.

We therefore measured ^1H CEST profiles for A_6 -DNA at 45°C (Fig. S2), in which the ssDNA population is $\sim 10\%$ (Shi et al., 2019). We did not observe any evidence for the ssDNA species in the ^1H CEST profiles. Instead, we were able to observe ultra-fast ($k_{\text{ex}} \sim 10\,000 \text{ s}^{-1}$, see Table S1) Hoogsteen exchange which could not previously be detected by ^{13}C or ^{15}N RD experiments at the same temperature (Shi et al., 2019).

Taken together, these results demonstrate that the ^1H CEST experiment broadens the range of populations and exchange rates over which Hoogsteen breathing can be effectively characterized.

3 Discussion

Building on prior studies showing the utility of the SELOPE ^1H RD experiment in measuring conformational exchange in unlabeled RNA (Schlagintweit et al., 2018) and DNA (Furukawa et al., 2021; Dubini et al., 2020), our study establishes the utility of high-power ^1H CEST SELOPE as a facile means for rapidly assessing the Watson–Crick to Hoogsteen exchange process in nucleic acids without the need for isotopic enrichment. The methodology is supported by the very good agreement observed between the measured exchange parameters and values measured independently using ^{13}C and/or ^{15}N $R_{1\rho}$ for a variety of bp's in three duplexes under different conditions of temperature and pH, as well as by the good agreement seen between the imino ^1H chemical shifts and those expected based on duplexes containing Hoogsteen bp's as the dominant GS conformation. The high throughput nature of the experiment and simple sample requirements enabled us to measure Hoogsteen dynamics for 37 data points corresponding to 22 distinct bp's for three different pH conditions and seven different temperatures (Table S1), the largest collection of Hoogsteen dynamics from a single study to date. We envision using the ^1H CEST SELOPE experiments to pre-screen DNA duplexes and to perform follow-up ^{13}C and ^{15}N RD experiments to confirm any interesting outliers, particularly regions showing substantially elevated Hoogsteen dynamics.

An important consideration when applying ^1H CEST to the study of chemical exchange are contributions due to ^1H – ^1H cross-relaxation originating from cross-relaxation, which may give rise to extraneous NOE dips that complicate data

analysis (Yuwen et al., 2017a; Bouvignies and Kay, 2012; Eichmuller and Skrynnikov, 2005). These contributions have been shown to be significant in proteins particularly when characterizing slow exchange ($k_{\text{ex}} < 200 \text{ s}^{-1}$) necessitating use of relatively long relaxation delays (Bouvignies and Kay, 2012). Consistent with prior studies of nucleic acids (Schlagintweit et al., 2018; Steiner et al., 2016; Baronti et al., 2020) and proteins (Lundstrom and Akke, 2005). Our results indicate that NOE effects from cross-relaxation between imino and non-imino protons can be effectively suppressed for DNA and RNA duplexes in the ^1H CEST experiments through selective excitation provided that the relaxation delays are short on the order of 100 ms (Fig. 3b). However, care should be exercised to assess imino–imino NOE effects (Fig. 3b), which may also be more substantial for certain non-canonical motifs. Data should be discarded if the ES chemical shifts match those of nearby imino protons identified using 2D [^1H , ^1H] NOESY experiments or if the magnitude of the dip of interest varies substantially with or without selective excitation, as this could be an indication of NOE effect. Finally, we recommend independent verification of the exchange parameters with the use of other methods such as ^{13}C and ^{15}N experiments for motifs exhibiting highly unusual exchange parameters or ES ^1H chemical shifts, and this can also help to confirm Hoogsteen bp's as the ES.

Prior studies showed that Watson–Crick to Hoogsteen bp transitions exhibit large variations in the forward rate constants (k_1), while the backward rate constants (k_{-1}) are relatively constant across different sequence contexts, consistent with a late transitional state (Alvey et al., 2014). We observe a similar trend in which k_{-1} varied < 5 -fold, while k_1 varied by ~ 50 -fold (Fig. S9). The ^1H CEST data also revealed significantly lower Hoogsteen abundance ($p_{\text{ES}} < 0.1\%$) in addition to slower exchange kinetics ($k_{\text{ex}} \sim 1000 \text{ s}^{-1}$) within A-tract motifs (Nikolova et al., 2011; Alvey et al., 2014) while also reinforcing prior data (Xu et al., 2018), suggesting increased exchange kinetics near terminal ends. Collectively, these data show that the Hoogsteen population can vary by as much as ~ 14 -fold, while k_{ex} can vary by ~ 20 -fold only due to changes in sequence and positional context (Table S1). These strong sequence and position dependencies could play important roles in biochemical processes acting on DNA.

A recent study (Furukawa et al., 2021) reported on-resonance imino ^1H $R_{1\rho}$ RD for a guanine residue in a DNA duplex at $\text{pH} = 7.5$, $T = 30^\circ\text{C}$, and in 150 mM NaCl. Because off-resonance measurements were not performed, only $k_{\text{ex}} \sim 10\,000 \text{ s}^{-1}$ could be determined, while the values of $\Delta\omega$ and p_{ES} were not determined. The study noted that a Hoogsteen bp as the ES was unlikely given that G–C⁺ Hoogsteen bp's are disfavored at $\text{pH} = 7.5$ and because the observed rate of exchange ($k_{\text{ex}} \sim 10\,000 \text{ s}^{-1}$) was much faster than is typically observed for Watson–Crick to Hoogsteen exchange. Instead, the data were interpreted as evidence for a base opened state. However, the observed rate of exchange $k_{\text{ex}} \sim 10\,000 \text{ s}^{-1}$ falls comfortably within the range of val-

ues measured here for Watson–Crick to Hoogsteen exchange using ^1H CEST at similar pH conditions. For example, for the G10–C15 bp's in A₆-DNA at the same temperature and $\text{pH} = 6.8$, k_{ex} for Watson–Crick to Hoogsteen exchange was $\sim 6000 \text{ s}^{-1}$ (Fig. 4 and Table S1). Similar Watson–Crick to Hoogsteen exchange parameters ($p_{\text{ES}} \sim 0.05\%$ and $k_{\text{ex}} \sim 2000 \text{ s}^{-1}$) were recently reported for this bp at 25°C and $\text{pH} 6.8$ using cytosine amino ^{15}N RD (Rangadurai et al., 2019a), and the ES $\Delta\omega_{\text{C-N4}} = -9$ ppm was shown to be in excellent agreement with values expected for a G–C⁺ Hoogsteen bp. In addition, based on hydrogen exchange measurements, $p_{\text{ES}} \sim 0.00001\%$ to 0.01% and k_{ex} ($k_{\text{cl}} + k_{\text{op}}$, k_{cl} and k_{op} are the base closing and opening rate constant, respectively) $\sim 10^5$ to 10^7 s^{-1} for the base-opened ES, and this process should fall outside RD detection (Gueron and Leroy, 1995; Gueron et al., 1987; Leroy et al., 1988; Leijon and Graslund, 1992; Snoussi and Leroy, 2001). Therefore, the ES detected by Furukawa et al. (2021) is more likely a Hoogsteen bp.

In conclusion, by obviating the need for isotopic enrichment, the ^1H CEST experiment expands the scope of characterizing Watson–Crick to Hoogsteen exchange in nucleic acids by NMR. We are presently applying the experiment to map the sequence dependence of Hoogsteen breathing dynamics and systematically, how it varies with pH, salt and crowding, and following the introduction of lesions, mismatches and molecules that bind to the DNA.

4 Methods

4.1 Sample preparation

Unlabeled DNA and RNA oligonucleotides. Unmodified DNA oligonucleotides were purchased from Integrated DNA Technologies with standard desalting purification. RNA oligonucleotides were synthesized using a MerMade 6 Oligo Synthesizer employing 2'-tBDSilyl protected phosphoramidites (*n*-acetyl protected rC, rA and rG, and rU phosphoramidites were purchased from ChemGenes) and 1 μmol standard synthesis columns (1000 Å) (BioAutomation). RNA oligonucleotides were synthesized with the final 5'-protecting group, 4,4'-dimethoxytrityl (DMT) retained. RNA oligonucleotides were cleaved from columns using 1 mL AMA (1 : 1 ratio of 30% ammonium hydroxide and 30% methylamine) and incubated at room temperature for 2 h. The sample was then air-dried and dissolved in 115 μL DMSO, 60 μL TEA, and 75 μL TEA.3HF, and then incubated at $T = 65^\circ\text{C}$ for 2.5 h to remove 2'-O protecting groups. The Glen-Pak RNA cartridges (Glen Research Corporation) were then used to purify the samples followed by ethanol precipitation.

Labeled DNA oligonucleotides. The uniformly ^{13}C , ^{15}N -labeled A₆-DNA sample was prepared using chemically synthesized DNA (purchased from IDT), Klenow fragment DNA polymerase (New England Biolab) and ^{13}C / ^{15}N iso-

topically labeled dNTPs (Silantes) using the Zimmer and Crothers method (Zimmer and Crothers, 1995). The oligonucleotide was purified using 20 % 29 : 1 polyacrylamide denaturing gel with 8 M urea, 20 mM Tris borate and 1 mM EDTA, and then using electro-elution (Whatman, GE Healthcare) in 40 mM Tris acetate and 1 mM EDTA, followed by ethanol precipitation.

Sample annealing and buffer exchange. DNA/RNA oligonucleotides were re-suspended in water (200–500 μM). To prepare duplex samples, equimolar amounts of the constituent single-stranded DNA/RNA samples were mixed and then heated at $T = 95^\circ\text{C}$ for ~ 5 min followed by cooling at room temperature for ~ 1 h. All samples were exchanged three times into the desired buffer using centrifugal concentrators (4 mL, Millipore Sigma). A total of 10 % D_2O (Millipore Sigma) was added to the samples prior to the NMR measurements.

Sample concentrations and buffer conditions. Unless mentioned otherwise, the NMR buffer contains 25 mM sodium chloride, 15 mM sodium phosphate, 0.1 mM EDTA and 10 % D_2O . Sample concentrations and buffer pH are as follows: A_6 -DNA, 1.0 mM, pH 6.8; A_2 -DNA, 1.0 mM, pH 5.4; A_5 -DNA, 0.2 mM, pH 5.2; A_6 -RNA, 0.5 mM, pH 6.8. Concentration was estimated by measuring the absorbance of the sample at 260 nm and using extinction coefficients from the ADT Biol Oligo calculator (<https://www.atdbio.com/tools/oligo-calculator>, last access: 12 September 2021).

4.2 NMR spectroscopy

All NMR experiments were performed on a 600 Bruker Avance 3 spectrometer equipped with a triple-resonance HCN cryogenic probe. The NMR data were processed and analyzed with NMRPipe (Delaglio et al., 1995) and SPARKY (Thomas D. Goddard and Donald G. Kneller, SPARKY 3, University of California, San Francisco).

Resonance assignments. Imino resonances were assigned using a combination of 2D [^1H , ^1H] NOESY and [^{15}N , ^1H] SOFAST-HMQC (Sathyamoorthy et al., 2014) experiments. Assignments for A_6 -DNA, A_2 -DNA and A_6 -RNA were reported previously (Sathyamoorthy et al., 2017; Zhou et al., 2016; Nikolova et al., 2011). The [^1H , ^1H] NOESY spectrum for A_5 -DNA is shown in Fig. S1.

^1H CEST. The pulse sequence is shown in Fig. 1b and was adapted from Schlagnitweit et al. (2018). The g_1 gradient (Fig. 1b) destroys transverse ^1H magnetization prior to excitation of imino resonances. This helps to avoid any accidental offset dependence of the starting ^1H magnetization. Relaxation delays $T_{\text{EX}} = 100$ ms were used for all ^1H CEST measurements at low temperatures (5–30 $^\circ\text{C}$), while a shorter $T_{\text{EX}} = 80$ ms was used for high (45 $^\circ\text{C}$) temperature measurements. A longer $T_{\text{EX}} = 400$ ms was used to illustrate artifacts arising due to NOE dips (Fig. 3b). RF power and offset combinations used in the CEST measurements are given in Table S2. Calibration of RF field powers for the ^1H CEST

measurements was performed as described previously (Rangadurai et al., 2019b) using the same pulse sequence. Field inhomogeneity was also measured (Fig. S10) using the same sequence and the procedure as described previously (Guenneugues et al., 1999). ^1H inhomogeneity was measured by performing on-resonance ^1H CEST experiments on G2-H1 of A_6 -DNA, chosen as it does not experience conformational exchange. The longest relaxation delays used for the measurements were 10, 2, 1, 0.4, 0.1 and 0.04 s for RF fields 10, 50, 100, 200, 1000 and 4000 Hz, respectively. The resulting nutation curve was Fourier transformed and was fit to a Gaussian function (blue lines in Fig. S10) to extract the full width at half maximum, which was used for defining the inhomogeneity as described previously (Guenneugues et al., 1999). The selective pulse was set to be off (Fig. 3b) by replacing pulse a (Fig. 1b) with a non-selective ^1H hard 90° pulse. A total of 16 scans were used for A_6 -DNA (1.0 mM) at 5, 10, 20, 25, 30 $^\circ\text{C}$, and A_2 -DNA (1.0 mM) at 25 $^\circ\text{C}$. A total of 32 scans were used for A_6 -RNA (0.5 mM) at 25 $^\circ\text{C}$. A total of 64 scans were used for A_5 -DNA (0.2 mM) at 25 $^\circ\text{C}$ and for A_6 -DNA (1.0 mM) at 45 $^\circ\text{C}$.

Fitting of ^1H CEST data. When performing two-state CEST fitting with and without exchange, we restricted the offset to -6 to 6 ppm for the ^1H CEST experiment with relaxation delay ≤ 100 ms and to -3 to 3 ppm for experiments with relaxation delay = 400 ms, to obviate any potential effects from ^1H – ^1H cross-relaxation artifacts (Fig. 3b). Peak intensities of all imino protons in the 1D spectra as a function of RF power and offset frequency were extracted using NMRPipe (Delaglio et al., 1995). The peak intensity at a given RF power and offset is normalized by the average peak intensity over the triplicate CEST measurements with zero relaxation delay under the same RF power. The uncertainty in the measured peak intensity at each offset frequency and RF power combination was assumed to be equal to the standard deviation of the peak intensities for triplicate CEST experiments with zero relaxation delay under the same RF power (Zhao et al., 2014; Shi et al., 2019). CEST profiles were generated by plotting the normalized intensity as a function of offset $\Omega = \omega_{\text{RF}} - \omega_{\text{obs}}$, where ω_{obs} is the Larmor frequency of the observed resonance and ω_{RF} is the angular frequency of the applied RF field. RF field inhomogeneity (Fig. S10) was taken into account during CEST fitting as described previously (Rangadurai et al., 2020a). The normalized CEST profiles were then fit via numerical integration of the Bloch–McConnell (B–M) equations as described previously (Rangadurai et al., 2020a). Fitting of CEST profiles without exchange (Figs. 4, S2–S4) was performed by setting $p_{\text{ES}} = k_{\text{ex}} = \Delta\omega = 0$. Errors in exchange parameters were set to be equal to the fitting errors which were obtained as the square root of the diagonal elements of the covariance matrix. Reduced chi-square ($r\chi^2$) was calculated to assess the goodness of fit (Rangadurai et al., 2019b). Note that the variations in $r\chi^2$ values for different ^1H CEST profiles in Fig. 4 and Fig. S2–4 are most likely due to differences in

the quality of the NMR data and poor estimation of the real experimental uncertainty. The residual sum of squares (RSS) was computed as follows:

$$\text{RSS} = \sum_{i=1}^n \left(I_i^{\text{fit}} - I_i^{\text{exp}} \right)^2, \quad (1)$$

where I_i^{fit} and I_i^{exp} are the i th fit and experimentally measured intensity in the CEST profile respectively, and the summation is over all RF power and offset combinations (N).

Model selection for fits with and without exchange (Figs. 4, S2–S4) was performed by computing AIC and BIC weights as follows (Burnham and Anderson, 2004):

$$\text{AIC} = \begin{cases} N \ln \left(\frac{\text{RSS}}{N} \right) + 2K, & \text{when } \frac{N}{K} \geq 40 \\ N \ln \left(\frac{\text{RSS}}{N} \right) + 2K + \frac{2K(K+1)}{N-K-1}, & \text{when } \frac{N}{K} < 40 \end{cases} \quad (2)$$

$$\text{wAIC} = \frac{e^{-0.5\Delta\text{AIC}}}{1 + e^{-0.5\Delta\text{AIC}}} \quad (3)$$

$$\text{BIC} = N \ln \left(\frac{\text{RSS}}{N} \right) + K \ln(N) \quad (4)$$

$$\text{wBIC} = \frac{e^{-0.5\Delta\text{BIC}}}{1 + e^{-0.5\Delta\text{BIC}}}, \quad (5)$$

where K is the number of floating parameters when fitting, and $\Delta\text{AIC}/\Delta\text{BIC}$ are the differences between two AIC values (fitting without and with exchange). The AIC (wAIC_{+ex}) and BIC (wBIC_{+ex}) weights for fits with exchange are reported in Figs. 4 and S2–S4. The improvement in the fit was considered statistically significant if both wAIC_{+ex} and wBIC_{+ex} values are > 0.995 , and $r\chi^2$ is reduced with the inclusion of exchange. For some resonances, the improvement in the fit with exchange is statistically significant, but the resulting exchange parameters are not reliable and have large errors (see Figs. S2, S3). For T4 in A₅-DNA, $p_{\text{ES}} = 0.2 \pm 0.1\%$ measured using ^1H CEST was ~ 10 -fold smaller than $p_{\text{ES}} = 2.7 \pm 1.5\%$ measured previously using ^{15}N RD (Alvey et al., 2014), whereas k_{ex} ($\sim 3000 \text{ s}^{-1}$) was in good agreement. However, simulations show that due to the small $\Delta\omega$ for ^{15}N (~ 1 ppm) and fast exchange kinetics k_{ex} ($\sim 3000 \text{ s}^{-1}$) the p_{ES} and $\Delta\omega$ are not well-determined by the ^{15}N RD data (Fig. S6c). For this reason, this data point was excluded for ^1H CEST and $^{13}\text{C}/^{15}\text{N}$ RD comparison (Fig. 5a).

Off-resonance ^{13}C $R_{1\rho}$ relaxation dispersion. ^{13}C $R_{1\rho}$ experiments were performed using 1D $R_{1\rho}$ schemes as described previously (Nikolova et al., 2012a, 2011; Hansen et al., 2009). The spin-lock powers and offsets are listed in Table S3. The spin-lock was applied for a maximal duration < 60 ms to achieve $\sim 70\%$ loss of peak intensity at the end of relaxation delay. Off-resonance $R_{1\rho}$ profiles (Fig. S8) were generated by plotting $(R_2 + R_{\text{ex}}) = (R_{1\rho} - R_1 \cos^2\theta) / \sin^2\theta$, where θ is the angle between the effective field of the observed resonance and the z axis, as a function of $\Omega_{\text{eff}}/2\pi$, where $\Omega_{\text{eff}} = \omega_{\text{obs}} - \omega_{\text{RF}}$, where ω_{obs} is the Larmor frequency

of the spin and ω_{RF} is the carrier frequency of the applied spin-lock.

Fitting of ^{13}C $R_{1\rho}$ data. One-dimensional peak intensities were measured using NMRPipe (Delaglio et al., 1995). $R_{1\rho}$ values for a given spin-lock power and offset were calculated by fitting the intensities as a function of delay time to a mono-exponential decay (Kimsey et al., 2015). A Monte Carlo approach was used to calculate the uncertainties of $R_{1\rho}$ (Bothe et al., 2014). Alignment of initial magnetization during the Bloch–McConnell fitting was performed based on the $k_{\text{ex}}/\Delta\omega$ value (Rangadurai et al., 2019b). Chemical exchange parameters were obtained by fitting experimental $R_{1\rho}$ values to numerical solutions of a two-state Bloch–McConnell (B–M) equations (McConnell, 1958). A Monte Carlo approach was used to calculate the errors of exchange parameters (Bothe et al., 2014). Reduced chi-square ($r\chi^2$) was calculated to assess the goodness of fit (Rangadurai et al., 2019b).

4.3 Thermodynamic Analysis

The observed temperature dependence of k_1 , k_{-1} for the Watson–Crick to Hoogsteen exchange measuring using ^1H CEST was fit to a modified van 't Hoff equation that accounts for statistical compensation effects and assumes a smooth energy surface as described previously (Nikolova et al., 2011; Coman and Russu, 2005):

$$\ln \left(\frac{k_i(T)}{T} \right) = \ln \left(\frac{k_{\text{B}}\kappa}{h} \right) - \frac{\Delta G_i^{\circ T}(T_{\text{hm}})}{RT_{\text{hm}}} - \frac{\Delta H_i^{\circ T}}{R} \left(\frac{1}{T} - \frac{1}{T_{\text{hm}}} \right). \quad (6)$$

k_i ($i = 1, -1$) is the forward and backward rate constants, and $\Delta G_i^{\circ T}(T)$ and $\Delta H_i^{\circ T}$ are the free energy (at temperature T , in kelvin) and enthalpy of activation ($i = 1$) or deactivation ($i = -1$) respectively. R is the universal gas constant ($\text{kcal mol}^{-1} \text{ K}^{-1}$) and T_{hm} is the harmonic mean of the experimental temperatures (T_i in K) computed as $T_{\text{hm}} = n / \sum_{i=1}^n (1/T_i)$, k_{B} is the Boltzmann's constant (J K^{-1}), κ is the transmission coefficient (assumed to be unity), and h is the Planck constant (J s).

The goodness-of-fit indicator R^2 (coefficient of determination) (Fig. S6) between the measured and fitted rate constants was calculated as follows: $R^2 = 1 - \frac{\text{SS}_{\text{res}}}{\text{SS}_{\text{total}}}$, $\text{SS}_{\text{res}} = \sum (k_{i,\text{fit}} - k_{i,\text{exp}})^2$, $\text{SS}_{\text{total}} = \sum (k_{i,\text{exp}} - \overline{k_{i,\text{exp}}})^2$. $k_{i,\text{fit}}$ and $k_{i,\text{exp}}$ ($i = 1, -1$) are fitted and experimentally measured rate constants. $\overline{k_{i,\text{exp}}}$ is the mean of all $k_{i,\text{exp}}$. Errors of fitting for $\Delta G_i^{\circ T}$ and $\Delta H_i^{\circ T}$ were calculated as the square root of the diagonal elements of the covariance matrix. $T \Delta S_i^{\circ T}$ is calculated as $\Delta H_i^{\circ T} - \Delta G_i^{\circ T}$.

Code and data availability. The data that support this study are contained in the published article (Tables S1–S3) or are available from the corresponding author on reasonable request. The Python scripts for ^1H CEST data fitting are available at <https://github.com/alhashimilab/1H-CEST> (last access: 12 September 2021) (DOI: <https://doi.org/10.5281/zenodo.5502219>, Liu et al., 2021b).

Supplement. The supplement related to this article is available online at: <https://doi.org/10.5194/mr-2-715-2021-supplement>.

Author contributions. BL, AR and HMAH conceived the project and experimental design. BL, AR and HS prepared the samples and set up the imino ^1H CEST experiment. BL performed ^1H CEST experiments and data analysis. HS performed ^{13}C $R_{1\rho}$ experiments. HMAH, BL and AR wrote the manuscript with critical input from HS.

Competing interests. Hashim M. Al-Hashimi is a member of the editorial board of *Magnetic Resonance*.

Disclaimer. Publisher's note: Copernicus Publications remains neutral with regard to jurisdictional claims in published maps and institutional affiliations.

Special issue statement. This article is part of the special issue "Geoffrey Bodenhausen Festschrift". It is not associated with a conference.

Acknowledgements. We thank Katja Petzold for sharing the ^1H CEST pulse sequence. We thank Or Szekely for general input and Ainan Geng for help with the ^1H inhomogeneity measurements.

Financial support. This research has been supported by the National Institutes of Health (grant no. R01GM089846).

Review statement. This paper was edited by Fabien Ferrage and reviewed by two anonymous referees.

References

Afek, A., Shi, H., Rangadurai, A., Sahay, H., Senitzki, A., Xhani, S., Fang, M., Salinas, R., Mielko, Z., Pufall, M. A., Poon, G. M. K., Haran, T. E., Schumacher, M. A., Al-Hashimi, H. M., and Gordan, R.: DNA mismatches reveal conformational penalties in protein-DNA recognition, *Nature*, 587, 291–296, <https://doi.org/10.1038/s41586-020-2843-2>, 2020.

Aishima, J., Gitti, R. K., Noah, J. E., Gan, H. H., Schlick, T., and Wolberger, C.: A Hoogsteen base pair embedded in undistorted B-DNA, *Nucleic Acids Res.*, 30, 5244–5252, 2002.

Alvey, H. S., Gottardo, F. L., Nikolova, E. N., and Al-Hashimi, H. M.: Widespread transient Hoogsteen base pairs in canonical duplex DNA with variable energetics, *Nat. Commun.*, 5, 4786, <https://doi.org/10.1038/ncomms5786>, 2014.

Baronti, L., Guzzetti, I., Ebrahimi, P., Friebe Sandoz, S., Steiner, E., Schlagnitweit, J., Fromm, B., Silva, L., Fontana, C., Chen, A. A., and Petzold, K.: Base-pair conformational switch modulates miR-34a targeting of Sirt1 mRNA, *Nature*, 583, 139–144, <https://doi.org/10.1038/s41586-020-2336-3>, 2020.

Ben Imeddourene, A., Zargarian, L., Buckle, M., Hartmann, B., and Mauffret, O.: Slow motions in A.T rich DNA sequence, *Sci. Rep.*, 10, 19005, <https://doi.org/10.1038/s41598-020-75645-x>, 2020.

Bothe, J. R., Stein, Z. W., and Al-Hashimi, H. M.: Evaluating the uncertainty in exchange parameters determined from off-resonance R1rho relaxation dispersion for systems in fast exchange, *J. Magn. Reson.*, 244, 18–29, <https://doi.org/10.1016/j.jmr.2014.04.010>, 2014.

Bouvignies, G. and Kay, L. E.: Measurement of proton chemical shifts in invisible states of slowly exchanging protein systems by chemical exchange saturation transfer, *J. Phys. Chem. B*, 116, 14311–14317, <https://doi.org/10.1021/jp311109u>, 2012.

Burnham, K. P. and Anderson, D. R.: Multimodel inference – understanding AIC and BIC in model selection, *Sociol. Method. Res.*, 33, 261–304, <https://doi.org/10.1177/0049124104268644>, 2004.

Chen, B., LeBlanc, R., and Dayie, T. K.: SAM-II Riboswitch Samples at least Two Conformations in Solution in the Absence of Ligand: Implications for Recognition, *Angew. Chem. Int. Edit.*, 55, 2724–2727, <https://doi.org/10.1002/anie.201509997>, 2016.

Coman, D. and Russu, I. M.: A nuclear magnetic resonance investigation of the energetics of basepair opening pathways in DNA, *Biophys. J.*, 89, 3285–3292, <https://doi.org/10.1529/biophysj.105.065763>, 2005.

Czernek, J., Fiala, R., and Sklenar, V.: Hydrogen bonding effects on the (^{15}N and (^1H) shielding tensors in nucleic acid base pairs, *J. Magn. Reson.*, 145, 142–146, <https://doi.org/10.1006/jmre.2000.2091>, 2000.

Delaglio, F., Grzesiek, S., Vuister, G. W., Zhu, G., Pfeifer, J., and Bax, A.: NMRPipe: a multidimensional spectral processing system based on UNIX pipes, *J. Biomol. NMR*, 6, 277–293, <https://doi.org/10.1007/BF00197809>, 1995.

Dubini, R. C. A., Schon, A., Muller, M., Carell, T., and Rovio, P.: Impact of 5-formylcytosine on the melting kinetics of DNA by ^1H NMR chemical exchange, *Nucleic Acids Res.*, 48, 8796–8807, <https://doi.org/10.1093/nar/gkaa589>, 2020.

Eichmuller, C. and Skrynnikov, N. R.: A new amide proton R1rho experiment permits accurate characterization of microsecond time-scale conformational exchange, *J. Biomol. NMR*, 32, 281–293, <https://doi.org/10.1007/s10858-005-0658-y>, 2005.

Felsenfeld, G., Davies, D. R., and Rich, A.: Formation of a 3-Stranded Polynucleotide Molecule, *J. Am. Chem. Soc.*, 79, 2023–2024, <https://doi.org/10.1021/ja01565a074>, 1957.

Frank, A. T., Horowitz, S., Andricioaei, I., and Al-Hashimi, H. M.: Utility of ^1H NMR chemical shifts in determining RNA structure and dynamics, *J. Phys. Chem. B*, 117, 2045–2052, <https://doi.org/10.1021/jp310863c>, 2013.

Furukawa, A., Walinda, E., Arita, K., and Sugase, K.: Structural dynamics of double-stranded DNA with epigenome

- modification, *Nucleic Acids Res.*, 49, 1152–1162, <https://doi.org/10.1093/nar/gkaa1210>, 2021.
- Golovenko, D., Brauning, B., Vyas, P., Haran, T. E., Rozenberg, H., and Shakked, Z.: New Insights into the Role of DNA Shape on Its Recognition by p53 Proteins, *Structure*, 26, 1237–1250 e1236, <https://doi.org/10.1016/j.str.2018.06.006>, 2018.
- Guenneugues, M., Berthault, P., and Desvaux, H.: A method for determining B1 field inhomogeneity. Are the biases assumed in heteronuclear relaxation experiments usually underestimated?, *J. Magn. Reson.*, 136, 118–126, <https://doi.org/10.1006/jmre.1998.1590>, 1999.
- Guéron, M. and Leroy, J. L.: Studies of base pair kinetics by NMR measurement of proton exchange, *Methods Enzymol.*, 261, 383–413, [https://doi.org/10.1016/s0076-6879\(95\)61018-9](https://doi.org/10.1016/s0076-6879(95)61018-9), 1995.
- Guéron, M., Kochoyan, M., and Leroy, J. L.: A single mode of DNA base-pair opening drives imino proton exchange, *Nature*, 328, 89–92, <https://doi.org/10.1038/328089a0>, 1987.
- Hansen, A. L., Nikolova, E. N., Casiano-Negroni, A., and Al-Hashimi, H. M.: Extending the range of microsecond-to-millisecond chemical exchange detected in labeled and unlabeled nucleic acids by selective carbon R(Irho) NMR spectroscopy, *J. Am. Chem. Soc.*, 131, 3818–3819, <https://doi.org/10.1021/ja8091399>, 2009.
- Hansen, A. L., Lundstrom, P., Velyvis, A., and Kay, L. E.: Quantifying millisecond exchange dynamics in proteins by CPMG relaxation dispersion NMR using side-chain ^1H probes, *J. Am. Chem. Soc.*, 134, 3178–3189, <https://doi.org/10.1021/ja210711v>, 2012.
- Hoogsteen, K.: The Structure of Crystals Containing a Hydrogen-Bonded Complex of 1-Methylthymine and 9-Methyladenine, *Acta Crystallogr.*, 12, 822–823, <https://doi.org/10.1107/S0365110x59002389>, 1959.
- Hwang, T. L. and Shaka, A. J.: Water Suppression That Works – Excitation Sculpting Using Arbitrary Wave-Forms and Pulsed-Field Gradients, *J. Magn. Reson. Ser. A*, 112, 275–279, <https://doi.org/10.1006/jmra.1995.1047>, 1995.
- Ishima, R. and Torchia, D. A.: Extending the range of amide proton relaxation dispersion experiments in proteins using a constant-time relaxation-compensated CPMG approach, *J. Biomol. NMR*, 25, 243–248, <https://doi.org/10.1023/a:1022851228405>, 2003.
- Ishima, R., Wingfield, P. T., Stahl, S. J., Kaufman, J. D., and Torchia, D. A.: Using amide H-1 and N-15 transverse relaxation to detect millisecond time-scale motions in perdeuterated proteins: Application to HIV-1 protease, *J. Am. Chem. Soc.*, 120, 10534–10542, <https://doi.org/10.1021/ja981546c>, 1998.
- Juen, M. A., Wunderlich, C. H., Nussbaumer, F., Tollinger, M., Kontaxis, G., Konrat, R., Hansen, D. F., and Kreutz, C.: Excited States of Nucleic Acids Probed by Proton Relaxation Dispersion NMR Spectroscopy, *Angew. Chem. Int. Ed. Engl.*, 55, 12008–12012, <https://doi.org/10.1002/anie.201605870>, 2016.
- Kimsey, I. J., Petzold, K., Sathyamoorthy, B., Stein, Z. W., and Al-Hashimi, H. M.: Visualizing transient Watson-Crick-like mispairs in DNA and RNA duplexes, *Nature*, 519, 315–320, <https://doi.org/10.1038/nature14227>, 2015.
- Kimsey, I. J., Szymanski, E. S., Zahurancik, W. J., Shakya, A., Xue, Y., Chu, C. C., Sathyamoorthy, B., Suo, Z., and Al-Hashimi, H. M.: Dynamic basis for dG*dT misincorporation via tautomerization and ionization, *Nature*, 554, 195–201, <https://doi.org/10.1038/nature25487>, 2018.
- Kitayner, M., Rozenberg, H., Rohs, R., Suad, O., Rabinovich, D., Honig, B., and Shakked, Z.: Diversity in DNA recognition by p53 revealed by crystal structures with Hoogsteen base pairs, *Nat. Struct. Mol. Biol.*, 17, 423–429, <https://doi.org/10.1038/nsmb.1800>, 2010.
- Lam, S. L. and Chi, L. M.: Use of chemical shifts for structural studies of nucleic acids, *Prog. Nucl. Magn. Reson. Spectrosc.*, 56, 289–310, <https://doi.org/10.1016/j.pnmrs.2010.01.002>, 2010.
- Lane, A. N., Bauer, C. J., and Frenkiel, T. A.: Determination of conformational transition rates in the trp promoter by ^1H NMR rotating-frame T1 and cross-relaxation rate measurements, *Eur. Biophys. J.*, 21, 425–431, <https://doi.org/10.1007/BF00185870>, 1993.
- LeBlanc, R. M., Longhini, A. P., Tugarinov, V., and Dayie, T. K.: NMR probing of invisible excited states using selectively labeled RNAs, *J. Biomol. NMR*, 71, 165–172, <https://doi.org/10.1007/s10858-018-0184-3>, 2018.
- Leijon, M. and Graslund, A.: Effects of sequence and length on imino proton exchange and base pair opening kinetics in DNA oligonucleotide duplexes, *Nucleic Acids Res.*, 20, 5339–5343, <https://doi.org/10.1093/nar/20.20.5339>, 1992.
- Leroy, J. L., Kochoyan, M., Huynh-Dinh, T., and Guéron, M.: Characterization of base-pair opening in deoxynucleotide duplexes using catalyzed exchange of the imino proton, *J. Mol. Biol.*, 200, 223–238, [https://doi.org/10.1016/0022-2836\(88\)90236-7](https://doi.org/10.1016/0022-2836(88)90236-7), 1988.
- Ling, H., Boudsocq, F., Plosky, B. S., Woodgate, R., and Yang, W.: Replication of a cis-syn thymine dimer at atomic resolution, *Nature*, 424, 1083–1087, <https://doi.org/10.1038/nature01919>, 2003.
- Liu, B., Shi, H., Rangadurai, A., Nussbaumer, F., Chu, C.-C., Erharter, K. A., Case, D. A., Kreutz, C., and Al-Hashimi, H. M.: A quantitative model predicts how m6A reshapes the kinetic landscape of nucleic acid hybridization and conformational transitions, *Nat. Commun.*, 12, 5201, <https://doi.org/10.1038/s41467-021-25253-8>, 2021a.
- Liu, B., Rangadurai, A., Shi, H., and Al-Hashimi, H.: Rapid measurement of Watson-Crick to Hoogsteen exchange in unlabeled DNA duplexes using high-power SELOPE imino ^1H CEST, Bei-1205/ ^1H -CEST, Zenodo [data set], <https://doi.org/10.5281/zenodo.5502219>, 2021b.
- Lu, L., Yi, C., Jian, X., Zheng, G., and He, C.: Structure determination of DNA methylation lesions N1-meA and N3-meC in duplex DNA using a cross-linked protein-DNA system, *Nucleic Acids Res.*, 38, 4415–4425, <https://doi.org/10.1093/nar/gkq129>, 2010.
- Lundstrom, P. and Akke, M.: Off-resonance rotating-frame amide proton spin relaxation experiments measuring microsecond chemical exchange in proteins, *J. Biomol. NMR*, 32, 163–173, <https://doi.org/10.1007/s10858-005-5027-3>, 2005.
- Lundstrom, P., Hansen, D. F., Vallurupalli, P., and Kay, L. E.: Accurate measurement of alpha proton chemical shifts of excited protein states by relaxation dispersion NMR spectroscopy, *J. Am. Chem. Soc.*, 131, 1915–1926, <https://doi.org/10.1021/ja807796a>, 2009.
- McConnell, H. M.: Reaction Rates by Nuclear Magnetic Resonance, *J. Chem. Phys.*, 28, 430–431, <https://doi.org/10.1063/1.1744152>, 1958.
- Nair, D. T., Johnson, R. E., Prakash, L., Prakash, S., and Aggarwal, A. K.: Hoogsteen base pair formation promotes synthesis opposite the 1,N6-ethenodeoxyadenosine lesion by human

- DNA polymerase *iota*, *Nat. Struct. Mol. Biol.*, 13, 619–625, <https://doi.org/10.1038/nsmb1118>, 2006.
- Nikolova, E. N., Kim, E., Wise, A. A., O'Brien, P. J., Andricioaei, I., and Al-Hashimi, H. M.: Transient Hoogsteen base pairs in canonical duplex DNA, *Nature*, 470, 498–502, <https://doi.org/10.1038/nature09775>, 2011.
- Nikolova, E. N., Gottardo, F. L., and Al-Hashimi, H. M.: Probing transient Hoogsteen hydrogen bonds in canonical duplex DNA using NMR relaxation dispersion and single-atom substitution, *J. Am. Chem. Soc.*, 134, 3667–3670, <https://doi.org/10.1021/ja2117816>, 2012a.
- Nikolova, E. N., Bascom, G. D., Andricioaei, I., and Al-Hashimi, H. M.: Probing Sequence-Specific DNA Flexibility in A-Tracts and Pyrimidine-Purine Steps by Nuclear Magnetic Resonance C-13 Relaxation and Molecular Dynamics Simulations, *Biochemistry*, 51, 8654–8664, <https://doi.org/10.1021/bi3009517>, 2012b.
- Nikolova, E. N., Goh, G. B., Brooks, C. L., 3rd, and Al-Hashimi, H. M.: Characterizing the protonation state of cytosine in transient G.C Hoogsteen base pairs in duplex DNA, *J. Am. Chem. Soc.*, 135, 6766–6769, <https://doi.org/10.1021/ja400994e>, 2013a.
- Nikolova, E. N., Zhou, H., Gottardo, F. L., Alvey, H. S., Kimsey, I. J., and Al-Hashimi, H. M.: A historical account of Hoogsteen base-pairs in duplex DNA, *Biopolymers*, 99, 955–968, <https://doi.org/10.1002/bip.22334>, 2013b.
- Otten, R., Villali, J., Kern, D., and Mulder, F. A.: Probing microsecond time scale dynamics in proteins by methyl (1)H Carr-Purcell-Meiboom-Gill relaxation dispersion NMR measurements. Application to activation of the signaling protein NtrC(r), *J. Am. Chem. Soc.*, 132, 17004–17014, <https://doi.org/10.1021/ja107410x>, 2010.
- Palmer III, A. G.: Chemical exchange in biomacromolecules: past, present, and future, *J. Magn. Reson.*, 241, 3–17, <https://doi.org/10.1016/j.jmr.2014.01.008>, 2014.
- Rangadurai, A., Zhou, H., Merriman, D. K., Meiser, N., Liu, B., Shi, H., Szymanski, E. S., and Al-Hashimi, H. M.: Why are Hoogsteen base pairs energetically disfavored in A-RNA compared to B-DNA?, *Nucleic Acids Res.*, 46, 11099–11114, <https://doi.org/10.1093/nar/gky885>, 2018.
- Rangadurai, A., Kremser, J., Shi, H., Kreutz, C., and Al-Hashimi, H. M.: Direct evidence for (G)O6H2-N4(C)(+) hydrogen bonding in transient G(syn)-C(+) and G(syn)-m(5)C(+) Hoogsteen base pairs in duplex DNA from cytosine amino nitrogen off-resonance R1rho relaxation dispersion measurements, *J. Magn. Reson.*, 308, 106589, <https://doi.org/10.1016/j.jmr.2019.106589>, 2019a.
- Rangadurai, A., Szymanski, E. S., Kimsey, I. J., Shi, H., and Al-Hashimi, H. M.: Characterizing micro-to-millisecond chemical exchange in nucleic acids using off-resonance R1rho relaxation dispersion, *Prog. Nucl. Magn. Reson. Spectrosc.*, 112–113, 55–102, <https://doi.org/10.1016/j.pnmrs.2019.05.002>, 2019b.
- Rangadurai, A., Shi, H., and Al-Hashimi, H. M.: Extending the Sensitivity of CEST NMR Spectroscopy to Micro-to-Millisecond Dynamics in Nucleic Acids Using High-Power Radio-Frequency Fields, *Angew. Chem. Int. Ed. Engl.*, 59, 11262–11266, <https://doi.org/10.1002/anie.202000493>, 2020a.
- Rangadurai, A., Shi, H., Xu, Y., Liu, B., Abou Assi, H., Zhou, H., Kimsey, I., and Al-Hashimi, H.: delta-Melt: Nucleic acid conformational penalties from melting experiments, *bioRxiv*, <https://doi.org/10.1101/2020.12.26.424438>, 2020b.
- Sathyamoorthy, B., Lee, J., Kimsey, I., Ganser, L. R., and Al-Hashimi, H.: Development and application of aromatic [(13)C, (1)H] SOFAST-HMQC NMR experiment for nucleic acids, *J. Biomol. NMR*, 60, 77–83, <https://doi.org/10.1007/s10858-014-9856-9>, 2014.
- Sathyamoorthy, B., Shi, H., Zhou, H., Xue, Y., Rangadurai, A., Merriman, D. K., and Al-Hashimi, H. M.: Insights into Watson-Crick/Hoogsteen breathing dynamics and damage repair from the solution structure and dynamic ensemble of DNA duplexes containing m1A, *Nucleic Acids Res.*, 45, 5586–5601, <https://doi.org/10.1093/nar/gkx186>, 2017.
- Schlagintweit, J., Steiner, E., Karlsson, H., and Petzold, K.: Efficient Detection of Structure and Dynamics in Unlabeled RNAs: The SELOPE Approach, *Chemistry*, 24, 6067–6070, <https://doi.org/10.1002/chem.201800992>, 2018.
- Schnieders, R., Wolter, A. C., Richter, C., Wohnert, J., Schwalbe, H., and Furtig, B.: Novel (13) C-detected NMR Experiments for the Precise Detection of RNA Structure, *Angew. Chem. Int. Ed. Engl.*, 58, 9140–9144, <https://doi.org/10.1002/anie.201904057>, 2019.
- Sekhar, A., Rosenzweig, R., Bouvignies, G., and Kay, L. E.: Hsp70 biases the folding pathways of client proteins, *Proc. Natl. Acad. Sci. USA*, 113, 2794–2801, <https://doi.org/10.1073/pnas.1601846113>, 2016.
- Shi, H., Clay, M. C., Rangadurai, A., Sathyamoorthy, B., Case, D. A., and Al-Hashimi, H. M.: Atomic structures of excited state A-T Hoogsteen base pairs in duplex DNA by combining NMR relaxation dispersion, mutagenesis, and chemical shift calculations, *J. Biomol. NMR*, 70, 229–244, <https://doi.org/10.1007/s10858-018-0177-2>, 2018.
- Shi, H., Liu, B., Nussbaumer, F., Rangadurai, A., Kreutz, C., and Al-Hashimi, H. M.: NMR Chemical Exchange Measurements Reveal That N(6)-Methyladenosine Slows RNA Annealing, *J. Am. Chem. Soc.*, 141, 19988–19993, <https://doi.org/10.1021/jacs.9b10939>, 2019.
- Shi, H., Kimsey, I., Liu, H., Pham, U., Schumacher, M. A., and Al-Hashimi, H.: Revealing A-T and G-C Hoogsteen base pairs in stressed protein-bound duplex DNA, *bioRxiv*, <https://doi.org/10.1101/2021.06.05.447203>, 2021.
- Singh, U. S., Moe, J. G., Reddy, G. R., Weisenseel, J. P., Marnett, L. J., and Stone, M. P.: 1H NMR of an oligodeoxynucleotide containing a propanodeoxyguanosine adduct positioned in a (CG)3 frameshift hotspot of Salmonella typhimurium hisD3052: Hoogsteen base-pairing at pH 5.8, *Chem. Res. Toxicol.*, 6, 825–836, <https://doi.org/10.1021/tx00036a012>, 1993.
- Smith, C. A., Ban, D., Pratihari, S., Giller, K., Schwiegk, C., de Groot, B. L., Becker, S., Griesinger, C., and Lee, D.: Population shuffling of protein conformations, *Angew. Chem. Int. Ed. Engl.*, 54, 207–210, <https://doi.org/10.1002/anie.201408890>, 2015.
- Snoussi, K. and Leroy, J. L.: Imino proton exchange and base-pair kinetics in RNA duplexes, *Biochemistry*, 40, 8898–8904, <https://doi.org/10.1021/bi010385d>, 2001.
- Sripakdeevong, P., Cevcec, M., Chang, A. T., Erat, M. C., Ziegeler, M., Zhao, Q., Fox, G. E., Gao, X., Kennedy, S. D., Kierzek, R., Nikonowicz, E. P., Schwalbe, H., Sigel, R. K., Turner, D. H., and Das, R.: Structure determination of noncanonical RNA motifs guided by (1)H NMR chemical shifts, *Nat. Methods*, 11, 413–416, <https://doi.org/10.1038/nmeth.2876>, 2014.

- Steiner, E., Schlagnitweit, J., Lundstrom, P., and Petzold, K.: Capturing Excited States in the Fast-Intermediate Exchange Limit in Biological Systems Using (HNMR)-H-1 Spectroscopy, *Angew. Chem. Int. Edit.*, 55, 15869–15872, <https://doi.org/10.1002/anie.201609102>, 2016.
- Stelling, A. L., Xu, Y., Zhou, H., Choi, S. H., Clay, M. C., Meriman, D. K., and Al-Hashimi, H. M.: Robust IR-based detection of stable and fractionally populated G-C(+) and A-T Hoogsteen base pairs in duplex DNA, *FEBS Lett.*, 591, 1770–1784, <https://doi.org/10.1002/1873-3468.12681>, 2017.
- Swails, J., Zhu, T., He, X., and Case, D. A.: AFNMR: automated fragmentation quantum mechanical calculation of NMR chemical shifts for biomolecules, *J. Biomol. NMR*, 63, 125–139, <https://doi.org/10.1007/s10858-015-9970-3>, 2015.
- Tateishi-Karimata, H., Nakano, M., and Sugimoto, N.: Comparable stability of Hoogsteen and Watson-Crick base pairs in ionic liquid choline dihydrogen phosphate, *Sci. Rep.*, 4, 3593, <https://doi.org/10.1038/srep03593>, 2014.
- Ughetto, G., Wang, A. H., Quigley, G. J., van der Marel, G. A., van Boom, J. H., and Rich, A.: A comparison of the structure of echinomycin and triostin A complexed to a DNA fragment, *Nucleic Acids Res.*, 13, 2305–2323, <https://doi.org/10.1093/nar/13.7.2305>, 1985.
- Wang, A. H., Ughetto, G., Quigley, G. J., Hakoshima, T., van der Marel, G. A., van Boom, J. H., and Rich, A.: The molecular structure of a DNA-triostin A complex, *Science*, 225, 1115–1121, <https://doi.org/10.1126/science.6474168>, 1984.
- Wang, S., Song, Y., Wang, Y., Li, X., Fu, B., Liu, Y., Wang, J., Wei, L., Tian, T., and Zhou, X.: The m(6)A methylation perturbs the Hoogsteen pairing-guided incorporation of an oxidized nucleotide, *Chem. Sci.*, 8, 6380–6388, <https://doi.org/10.1039/c7sc02340e>, 2017.
- Wang, Y., Han, G., Jiang, X., Yuwen, T., and Xue, Y.: Chemical shift prediction of RNA imino groups: application toward characterizing RNA excited states, *Nat. Commun.*, 12, 1595, <https://doi.org/10.1038/s41467-021-21840-x>, 2021.
- Wang, Y. S. and Ikuta, S.: Proton on-Resonance Rotating Frame Spin-Lattice Relaxation Measurements of B and Z Double-Helical Oligodeoxyribonucleotides in Solution, *J. Am. Chem. Soc.*, 111, 1243–1248, <https://doi.org/10.1021/ja00186a013>, 1989.
- Weininger, U., Liu, Z., McIntyre, D. D., Vogel, H. J., and Akke, M.: Specific $^{12}\text{C}_{\beta\text{D}(2)}^{12}\text{C}_{\gamma\text{D}(2)}^{13}\text{C}_{\epsilon\text{HD}(2)}$ isotopomer labeling of methionine to characterize protein dynamics by ^1H and ^{13}C NMR relaxation dispersion, *J. Am. Chem. Soc.*, 134, 18562–18565, <https://doi.org/10.1021/ja309294u>, 2012.
- Weininger, U., Blissing, A. T., Hennig, J., Ahlner, A., Liu, Z., Vogel, H. J., Akke, M., and Lundstrom, P.: Protein conformational exchange measured by ^1H R ρ relaxation dispersion of methyl groups, *J. Biomol. NMR*, 57, 47–55, <https://doi.org/10.1007/s10858-013-9764-4>, 2013.
- Xu, Y., McSally, J., Andricioaei, I., and Al-Hashimi, H. M.: Modulation of Hoogsteen dynamics on DNA recognition, *Nat. Commun.*, 9, 1473, <https://doi.org/10.1038/s41467-018-03516-1>, 2018.
- Xu, Y., Manghrani, A., Liu, B., Shi, H., Pham, U., Liu, A., and Al-Hashimi, H. M.: Hoogsteen base pairs increase the susceptibility of double-stranded DNA to cytotoxic damage, *J. Biol. Chem.*, 295, 15933–15947, <https://doi.org/10.1074/jbc.RA120.014530>, 2020.
- Yamazaki, T., Muhandiram, R., and Kay, L. E.: NMR Experiments for the Measurement of Carbon Relaxation Properties in Highly Enriched, Uniformly ^{13}C , ^{15}N -Labeled Proteins: Application to ^{13}C .alpha. Carbons, *J. Am. Chem. Soc.*, 116, 8266–8278, <https://doi.org/10.1021/ja00097a037>, 1994.
- Yuwen, T., Sekhar, A., and Kay, L. E.: Separating Dipolar and Chemical Exchange Magnetization Transfer Processes in (1) H-CEST, *Angew. Chem. Int. Ed. Engl.*, 56, 6122–6125, <https://doi.org/10.1002/anie.201610759>, 2017a.
- Yuwen, T. R., Huang, R., and Kay, L. E.: Probing slow timescale dynamics in proteins using methyl H-1 CEST, *J. Biomol. NMR*, 68, 215–224, <https://doi.org/10.1007/s10858-017-0121-x>, 2017b.
- Zhao, B., Hansen, A. L., and Zhang, Q.: Characterizing slow chemical exchange in nucleic acids by carbon CEST and low spin-lock field R(1rho) NMR spectroscopy, *J. Am. Chem. Soc.*, 136, 20–23, <https://doi.org/10.1021/ja409835y>, 2014.
- Zhou, H., Kimsey, I. J., Nikolova, E. N., Sathyamoorthy, B., Grazioli, G., McSally, J., Bai, T., Wunderlich, C. H., Kreutz, C., Andricioaei, I., and Al-Hashimi, H. M.: m(1)A and m(1)G disrupt A-RNA structure through the intrinsic instability of Hoogsteen base pairs, *Nat. Struct. Mol. Biol.*, 23, 803–810, <https://doi.org/10.1038/nsmb.3270>, 2016.
- Zhou, H., Sathyamoorthy, B., Stelling, A., Xu, Y., Xue, Y., Pigli, Y. Z., Case, D. A., Rice, P. A., and Al-Hashimi, H. M.: Characterizing Watson-Crick versus Hoogsteen Base Pairing in a DNA-Protein Complex Using Nuclear Magnetic Resonance and Site-Specifically (^{13}C - and (^{15}N)-Labeled DNA, *Biochemistry*, 58, 1963–1974, <https://doi.org/10.1021/acs.biochem.9b00027>, 2019.
- Zimmer, D. P. and Crothers, D. M.: NMR of enzymatically synthesized uniformly ^{13}C / ^{15}N -labeled DNA oligonucleotides, *Proc. Natl. Acad. Sci. USA*, 92, 3091–3095, <https://doi.org/10.1073/pnas.92.8.3091>, 1995.